

UCLA

UCLA Electronic Theses and Dissertations

Title

Nanoparticle Measurements in Parallel Artificial Bilayers

Permalink

<https://escholarship.org/uc/item/4ph6g11s>

Author

Smith, Tyler

Publication Date

2014

Peer reviewed|Thesis/dissertation

UNIVERSITY OF CALIFORNIA

Los Angeles

NANOPARTICLE MEASUREMENTS IN PARALLEL ARTIFICIAL BILAYERS

A thesis submitted in partial satisfaction

Of the requirements for the degree Master of Science

In Bioengineering

By

Tyler Scott Smith

2014

© Copyright by

Tyler Scott Smith

2014

ABSTRACT OF THE THESIS

By

Tyler Scott Smith

Master of Science in Bioengineering

University of California, Los Angeles, 2014

Professor Jacob Schmidt

Artificial lipid bilayers have had a long history in the investigation of ion channels and pore proteins. They have been well established as a viable method as a detection tool via pore protein sensing but lack the ability to quickly and efficiently collect statistically useful data using traditional platforms. The utilization of the droplet bilayer method in particular has had significant improvements in scalability and automation. The development of a high throughput platform is pivotal for collecting large volumes of experimental data and to obtain statistically relevant datasets. The work performed in this thesis utilizes experimental observations and modified fabrication techniques to establish a more efficient method of bilayer reconstitution. In addition, numerous protocols were developed for testing nanoparticles in artificial plasma and lysosomal membranes in mass quantities. This improved platform utilizes simple electrical measurements to quantify the interactions between various nanoparticles and artificial membranes at various concentrations, ionic strengths and pH values to better understand biological mechanisms of interaction. In addition, the added improvements bring this platform one step closer to large-scale sensing and screening applications.

The thesis of Tyler Scott Smith is approved.

Jacob Schmidt

Warren Grundfest

Gerard Wong

University of California, Los Angeles

2014

TABLE OF CONTENTS

LIST OF FIGURES	v
Acknowledgements	viii
CHAPTER 1: Introduction	1
CHAPTER 2: Reconstitution Methods	5
2.1 Painted Bilayers	5
2.2 Patch-Clamp Technique	8
2.3 Supported Bilayers	8
2.4 Droplet Bilayers	9
CHAPTER 3: High Throughput Platform	10
3.1 Chip Fabrication	10
3.2 Bilayer Formation	11
CHAPTER 4: Technology Innovations	15
4.1 Laser Characterization	15
4.2 Measurement Automation	18
Chapter 5: Current Applications	22
5.1 Nanoparticle Interaction	24
5.2 Artificial Physiological Membrane Compositions	28
5.3 High-Throughput Nanoparticle Studies	40
Chapter 6: Conclusions	51
Chapter 7: Future Applications	53
7.1 Nanoparticle Screening	53
7.2 Nanopore Sequencing	53
Appendix A. Protocols	56
References	60

LIST OF FIGURES

Figure 1. Experimental chambers for the formation of painted bilayers. The cylinder is placed within the larger apparatus (A) where the inner and outer wells can be accessed. The small aperture is located within the center of the circle (B). (Williams).....	6
Figure 2. A representative image of the aperture used for painted bilayers of roughly 250 μ m in diameter.	7
Figure 3. Current platform for bilayer parallelization schematic. [19]	10
Figure 4. Gramicidin channels confirming bilayer membrane formation.	14
Figure 5. A poorly formed aperture that resulted in an unstable bilayer during a previous experiment is observed under a 10X microscope for characterization.....	16
Figure 6. (Left) The juxtaposition of the result of reflected laser on aperture formation and a typical aperture produced by the laser cutter (right).	17
Figure 7. Acrylic film template designed for consistent aperture fabrication. Two quarter-inch acrylic plates sandwich a thin sheet of Delrin® film to elevate and hold the film above the laser cutting board.	18
Figure 8. (left) The diameter of the aperture measured by the yellow horizontal line and (right) the area of the aperture measured by the area within the yellow circle in Image].	19
Figure 9. A simplified view of a large influx of current as a result of an immediate bilayer fusion. (Left) a flat current reading centered at 0pA without any noise or leak currents observed. (Right) A fusion event observed by an influx of current and plateauing at the maximum current reading of 4000pA.....	24
Figure 10. An example of a nanoparticle interaction event where a transient pore formation and subsequent reformation of a stable bilayer membrane takes place.....	25
Figure 11. An example of the current used to quantify the transient pore size in a membrane.	26
Figure 12. (Left) Amine-modified nanoparticles interacting with a consistent dependence on the sign of the voltage sweep. The amine-modified nanoparticles consistently interact during the positive voltage sweep. (Right) An illustration of the location of nanoparticles relative to the electrode placement.	28
Figure 13. Bilayer fusion rate dependence on nanoparticle concentration and ionic strength.	34
Figure 14. Bilayer fusion rates as a function of pH and experimental condition. As the pH increases, the number of wells that exhibit a fusion event decreases for the experimental group.	37

Figure 15. Preliminary experimentation with C60 nanoparticles under plasma membrane conditions. **41**

Figure 16. Gd₂O₃ nanoparticle preliminary experiment data showing strong signs of interaction under plasma membrane conditions. **42**

Figure 17. Gd₂O₃ nanoparticles exhibiting strong signs of interaction under lysosomal membrane conditions. **43**

Figure 18. Platinum nanoparticles of 30nm diameter under plasma membrane conditions exhibit no significant signs of interaction events. **44**

Figure 19. Platinum nanoparticles of 5nm diameter under plasma membrane conditions exhibit no significant signs of interaction events. **45**

Figure 20. Platinum nanoparticles of 5nm diameter under lysosomal membrane conditions exhibit no significant signs of interaction events. **46**

Figure 21. Platinum nanoparticles of 30nm diameter under lysosomal membrane conditions exhibit no significant signs of interaction events. **47**

Figure 22. Repeated experiment confirming platinum nanoparticles of 30nm diameter under lysosomal membrane conditions do not exhibit any significant sign of interaction events. **48**

Figure 23. Preliminary experiment with iron oxide nanoparticles may show possible interaction events under lysosomal membrane conditions. **49**

LIST OF TABLES

Table 1. Bilayer formation and fusion rates before laser characterization.	15
Table 2. ImageJ aperture quantitative analysis protocol.	20
Table 3. A summary of the nanoparticle interaction data with pure POPE lipid membranes.	23
Table 4. Total brain lipid extract bilayers under plasma membrane conditions were tested using carboxyl and amine-modified polystyrene nanoparticles. *Noise currents associated likely from an unclean chip.....	29
Table 5. Total heart lipid extract bilayers under plasma membrane conditions were tested using amine-modified polystyrene nanoparticles.	31
Table 6. POPE lipid bilayers tested under various ionic strengths and concentrations of amine-modified and carboxyl-modified nanoparticles. *Noise currents associated likely from an unclean chip.	32
Table 7. Preliminary data comparing bilayer stability with two different buffer solutions and amine-modified nanoparticles.....	35
Table 8. Preliminary data illustrating the consistency and repeatability of data collection and test conditions.	36
Table 9. The most recently established composition of the plasma and lysosomal membranes on the basis of molar ratios of various lipids.	39
Table 10. Aqueous buffer solution compositions for the plasma and lysosomal membranes.	39

Acknowledgements

I would like to dedicate my thesis to my brother and best friend, Chandler. Your constant love and support will never go unnoticed. You have actively supported me in every endeavor I put my mind to. Thank you, I couldn't have made this journey without you.

There are a great number of people without whom this thesis might not have been written and to whom I will always be grateful for.

I would like to thank my committee members, Professor Jacob Schmidt, Professor Warren Grundfest and Professor Gerard Wong. Their commitments to education, both inside and out of the classroom have been truly invaluable.

To the two most influential professors in my life, it is with immense gratitude that I acknowledge the support and help of Dr. Jacob Schmidt for guiding my academic path throughout my endeavors at UCLA and graciously allowing me to join his lab. I would also like to give thanks to my undergraduate advisor and Professor, Dr. Trevor Cardinal, a dear friend and academic mentor. Without the guidance and patience of these two individuals, this thesis would not be possible. Thank you for your wisdom and kindness.

To my family, I would like to thank you for your love, support, guidance, patience and contribution to the experiences that have made me the person I am today. Thank you for never letting me settle for anything but my best in everything that I do.

To my father, Scott Smith, for teaching me to always take the time to “measure twice and cut once” and to treat everyone with kindness. As I have become older I have begun to understand

your sacrifices and commitment to both my education and character development and I don't know how to begin to thank you. The path to success is a limitless one but I know you will help me as you have always done, one step at a time.

To my dear mother, Tricia Smith, who has always encouraged me to follow my own path in life and for supporting me through all my successes and failures along the way. Your humility and selflessness is incredible. Thank you for putting up with me all these years and always reminding me that happiness is the only thing in life that truly matters.

To one of the closest friends I'll ever have, Shiv Acharya. Your kindness, loyalty, humor, morality, humility and pursuit of knowledge are second to none and it has been an honor to be your friend and partner-in-crime. You have accepted me for who I am and taught me a great deal about the world and what it means to be a true friend.

To my good friend and mentor, Bin Lu, your positive attitude and love of everything bilayers made my transition into graduate-level research very enjoyable. Thank you for being patient throughout my experience as a researcher and constantly answering my questions. You are certainly my better half in lab. Team bilayer: One Team, One Dream. Thank you, Sifu, I wish you all the best in finishing your doctorate.

To past and present members of the Schmidt lab, thank you for putting up with me. I'm certainly the catalyst of the group and I can definitely be the trouble-maker from time-to-time. I enjoyed every moment in lab with you all, both the good and the bad and I couldn't have worked with a better group of people. I couldn't have asked for a better work environment and I wish the best for all of you. You helped make my graduate experience something I will always cherish.

To one of my oldest friends, Brooke Wojdyski, who has individually taught me more than anyone else in my life about who I am. You have stuck around through my many phases and transitions in life and for that I thank you for never leaving; you grew up much quicker than I did and you were wise to be patient. I'm willing to bet you didn't think you would need to wait as long as you did but I am grateful you did. Thank you for your patience, laughter and love. Let's change the world together.

I would also like to acknowledge Dave Thuleen, for his academic guidance and years of friendship. You have gone far beyond the call of a teacher and have proven to be a wonderful addition to my life. Our conversations about physics, the universe and random thoughts over a cup of coffee or a glass of wine have been so delightful. You have shown me the beauty of science and the virtue in the pursuit of truth and knowledge.

CHAPTER 1: Introduction

Nanoparticles are at the forefront of the rapidly developing field of nanotechnology. Their sub-micron size offers unique applications in biology and medicine such as biological fluorescent labeling, drug and gene delivery, detection of proteins, tissue engineering, MRI contrast enhancement, and probing of DNA structures [1]. Nanoparticles exist on the size domain of proteins which makes them suitable for tagging or labeling. Size alone does not justify a nanoparticle as a relevant biological labeler; it is their ability to be altered with biological coatings such as antibodies or biopolymers that allow nanoparticles to become biocompatible. A unique application using nanoparticles is in drug delivery. Briefly, nanoparticles are loaded with active molecules and their surfaces are modified with a target-specific ligand used to reach an intended target. The nanoparticles are injected into the bloodstream and transported until it reaches the intended target at which point the ligand binds with an appropriate receptor and the active molecule contained within the nanoparticle is released [2]. Another important use for nanoparticles is in protein detection. Proteins are a critical aspect in cell-to-cell signaling, mechanical structure and basic cellular functions. Gold nanoparticles have been used in immunohistochemistry to identify specific protein-protein interactions [1]. With an abundance of nanoparticle sizes, shapes, charge and surface modifications available, the understanding of how these numerous particle configurations interact in biologically relevant systems has only recently been investigated. Hence, it is critical to develop a system by which these seemingly limitless combinations of nanoparticles can be tested and evaluated.

To simplify the investigation between the human body and the nanoparticles in question, a high-throughput artificial system is used to mimic the conditions in the basic structural unit of all living organisms, the cell. By creating this system, nanoparticle characteristics and cytotoxicity could be investigated in large, statistically relevant, data sets very quickly.

To create a platform for testing, it is important to understand the fundamental basics that comprise all human cells. Cells come in many sizes, shapes and compositions but one thing remains the same, a protective membrane that encapsulates each cell. These membranes serve as a protective barrier between the extracellular space and the lumen of the cell. The cell membrane is also critical to adhesion to other cells and cell signaling among other uses. Within the cell there is deeper organization; intracellular organelles, such as mitochondria and lysosomes, are compartmentalized by their own membranes, separate from the encapsulating membrane. The nature of these intracellular membranes reflects their purpose within the cell and fulfills a variety of functions. Each of these membranes creates a closed system; thus, a pathway for transportation and communication is required and this comes in the form of selectively permeable membrane proteins. Singer and Nicholson famously investigated the structure of biological membranes and established the “fluid mosaic model” which provided scientists with a model for basic membrane structure [3]. Simply put, the basic structure of biologically relevant membranes consists of phospholipids and embedded proteins [4]. Phospholipids are amphipathic, meaning they contain a hydrophilic “head” region in conjunction with a lipophilic tail region. When exposed to an oil-water interface, the lipids will orient themselves with the head group facing the aqueous phase and the tail region in the organic phase. This is referred to as the hydrophobic effect. In the case of all cells, the membrane is composed of two monolayers sandwiched together to form a bilayer with the head groups oriented radially with the tail groups of each layer facing each other to form the inside of the membrane. The nature of these bilayers creates a lipophilic region within the membrane, resulting in nearly impossible ion transport across the membrane via diffusion. The difficulty in diffusion-facilitated transportation across a membrane becomes evident here and the importance of embedded transport proteins becomes clear. The nature of these embedded proteins varies widely as some proteins are fixed within the

membrane and others passively diffuse. The plethora of protein types allows the cell and its multi-membrane system and organelles to very selectively regulate transportation and communication.

The impact of studying these pivotal structures is key to understanding how the body works from a cellular level and has been studied for many centuries since its discovery by Robert Hooke in 1665 [5] .

Unlike Hooke, who used a simple microscope to discover the first cell, our equipment utilizes highly sensitive electronic equipment to apply a voltage potential across the various membranes we create and record data in the form of amplified currents. More specifically, the formation of these membranes is monitored through an increase in capacitive current readings as measured by what is known as voltage clamp. Voltage clamp is a current measuring technique of excitable cells where the membrane voltage is set to a constant value. This set voltage can vary depending on experimental parameters and the type of membrane the experiment is trying to mimic. Cell membranes contain many ion channels, some of which are voltage-gated, meaning they are activated by changes in local electrical membrane potential. The voltage clamp can be manipulated independently of these ionic currents associated with the ion channels. Although very thin, typically around 5nm in diameter, the membrane is impermeable to water-soluble ions. This typically results in highly resistive membranes regularly measuring between $10^7 - 10^8 \Omega \cdot cm^2$. The basic lipid membrane is considered to constitute an ideal, electrically inert barrier to the movement of ions and some molecules [6]. The embedded proteins cause the cell membrane to become selectively permeable, thus controlling the movement of ions and organic compounds that leave and enter the cell. This selective permittivity also reduces the resistivity of the membrane in some cases on the order of $10^3 \Omega \cdot cm^2$ [7].

Assembling lipid bilayers is common to two basic methods: as small vesicles or as a single planar structure separating two aqueous phases. Each model has its own advantages and shortcomings. The vesicle model is advantageous for flux measurements and the lack of a hydrocarbon solvent may be a strong factor in the incorporation of membrane proteins during reconstitution. In contrast, their small size and inaccessible core result in difficult electrical measurements and chemical manipulation.

The latter method, and that of which this paper will discuss deeply, is planar lipid bilayers. This method offers access to both sides of the membrane for solution exchange and easy electrical measurements, perfect for our goal of parallelization and recording large data sets.

To further understand the platform and its uses it is best to start with the common and historical methods for creating lipid bilayers.

CHAPTER 2: Reconstitution Methods

2. 1 Painted Bilayers

The history of bilayer reconstitution methods has spanned nearly half a century. Numerous methods have been developed to study biological systems that would normally be very difficult to study, such as the nucleus of a cell or the endoplasmic reticulum. These structures lie deep within the cell and are electrically difficult to access on large scales. In this chapter, the traditional methods used to form bilayers and incorporated ion-channels will be briefly overviewed to better understand how the current method was established.

The first method depicts a simple apparatus with a two-chamber design with a small $\sim 200\mu\text{m}$ septum connecting the two chambers similar to the design shown in Figure 1. Prior to bilayer formation, the aperture is “primed” by applying a very small amount of phospholipid-oil solution. The film is then allowed to dry in a desiccator to expedite the process. Experimental buffer solutions are added to both chambers before what is referred to as “painting” can occur. When the solutions have settled, a pipette tip is dipped into the phospholipid-oil solution and then carefully drawn across the aperture. This painting motion gave rise to the name, painted bilayer method. This particular technique varies from lab-to-lab and the applicator can be a pipette tip, a brush or even a plastic rod depending on the user’s preference and protocol.

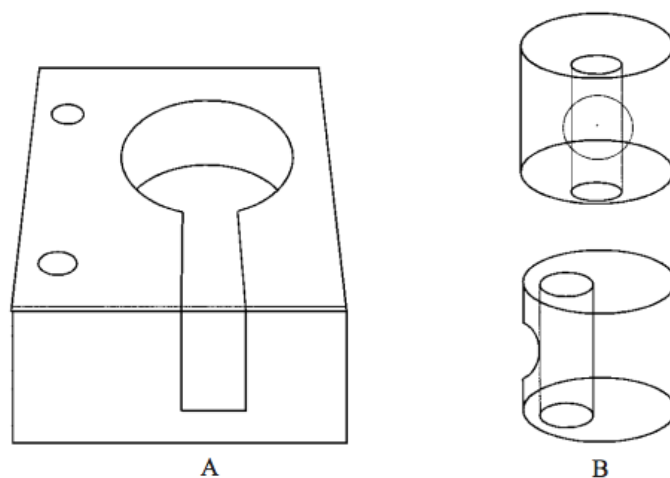


Figure 1. Experimental chambers for the formation of painted bilayers. The cylinder is placed within the larger apparatus (A) where the inner and outer wells can be accessed. The small aperture is located within the center of the circle (B). (Williams)

White et al. described the resulting film created by drawing the lipid-oil solution across the aperture as several microns thick and will thin spontaneously to form a bilayer membrane [8]. The spontaneous thinning is explained by the Plateau-Gibbs border suction. Briefly, as the film thins, the Van der Waals attraction between the aqueous phases on either side of the forming membrane contributes to the additional driving force, which continues to thin the membrane. Interestingly, the material from which the septum is made from has a drastic effect on the outcome of bilayer formation. Teflon has been a reliable material used to consistently form stable bilayers both in use in our platform as well as others. The material is important because it dictates how consistent the diameter and roundness of the aperture will be. The consistency of the size of the aperture is also critical because small holes, on the order of a few hundred microns and in some cases less than $100\mu\text{m}$ in diameter, have been shown to be difficult to form bilayers with [9]. This is likely due to a high aspect ratio, which makes film thinning very difficult.

To observe the thinning of the film and subsequent bilayer formation, observation under reflected light can give a quick qualitative answer to whether or not a bilayer has formed properly or not. Upon formation, the bilayer is roughly 50\AA thick and therefore reflects little to

no light and appears black. This observation gave rise to the nickname of black lipid membrane or BLM for short.

A representative image of the aperture used for painted bilayers can be seen below in Figure 2. The aperture diameter is roughly $250\mu\text{m}$ and the film is on the order of 30 to $50\mu\text{m}$ in thickness. This aspect ratio has shown to be effective in creating consistent painted bilayers. If the thickness and diameter are not critically taken into consideration during the fabrication process, the resulting apertures will not result in stable and consistent painted bilayers. The process used to create these apertures and platform technology will be discussed in a later chapter.

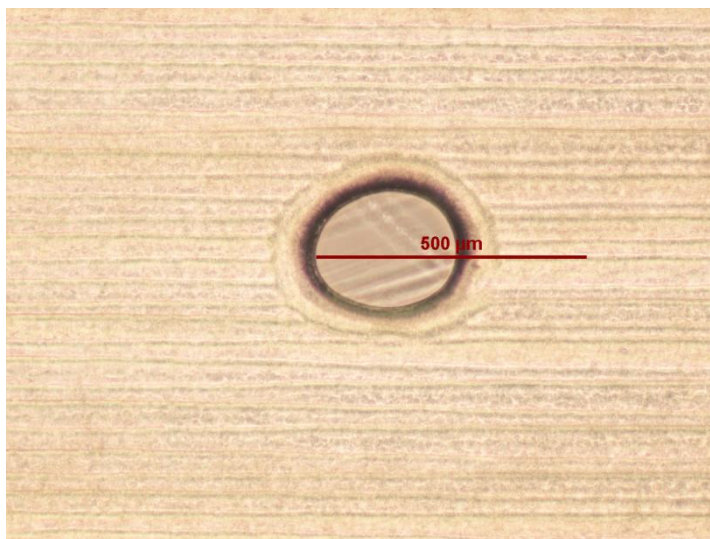


Figure 2. A representative image of the aperture used for painted bilayers of roughly $250\mu\text{m}$ in diameter.

In general, the method of painting bilayers is fairly simple and can be learned in a few hours. One major drawback to the painted bilayer method is the ability to create large numbers of bilayers in a short amount of time. The labor portion of painting bilayers can be tedious and is sensitive to vibration disturbances and is time consuming when compared to the droplet bilayer method. Another common problem associated with painted bilayers is the residual solvent

between the two monolayers which can disrupt protein function within the membrane and also limits the lifetime of the artificial bilayer membrane.

2.2 Patch-Clamp Technique

As briefly described in the introduction, biological membranes are complicated. Although various techniques and methods have been used to replicate these systems, there are many benefits to using the real plasma membrane of a living cell. The patch-clamp technique was developed by Sakmann and Neher in the early 1980's and brought forth a new technique for researchers to investigate real biological membranes [10]. This technique works on the premise that a very small area can be isolated via a small pipette tip. If the area of the pipette tip is small enough, generally on the order of microns, even a single protein can be investigated within a single membrane. By attaching this pipette tip to the membrane, via a light suction, the pipette can be electrically isolated from the rest of the cell. When the pipette tip is attached, it can then be pulled away from the membrane to detach a small "patch" of membrane. The advantage of patch clamp is its high reproducibility and electrical resolution; however, not all membranes can use this technique, such as those surrounding organelles and it is difficult to parallelize this system.

2.3 Supported Bilayers

One solution developed to address the short lifetime of previous bilayer lifetimes is the method of supported lipid bilayers. In this technique, a planar bilayer is supported via a substrate, typically a hydrogel such as agarose. The monolayer closest to the substrate is only separated by a very thin hydration layer, which keeps it from direct contact from the substrate material. By supporting the bilayer, the lifetime dramatically increases from hours to days and in some cases weeks. The main drawback of this model is the inability to use asymmetrical solutions.

2. 4 Droplet Bilayers

The method utilized in this platform involves the apposition of two phospholipid monolayers formed at a horizontal interface between two aqueous solutions and air [8]. The amphiphilic phospholipids will spontaneously orient themselves depending on the medium in which they are placed. In the case of an aqueous-air interface, the hydrophilic head group will orient toward the aqueous phase. This causes the formation of a single monolayer at the aqueous-air interface. By increasing the height of the solution within the chamber over the aperture, the monolayers on each side of the partition will begin to join together at the aperture to form a small bilayer. The resulting bilayer contains less solvent than the traditional painted bilayer method.

Takeuchi's group developed a micro-fabricated chip that supported the formation of 96 bilayers using eight multiplexed fluidic and electrical connections [11, 12]. His group was able to use this device to form 44 bilayers simultaneously, resulting in a 46% yield. They then developed another microfluidic device in which lipid bilayers were formed by contacting two monolayers which self-assembled at aqueous-oil interfaces [13]. This technique is referred to as the "droplet interface bilayers" method [14-16]. This method was viewed as a technological advantage to previous techniques because the only complication in the system relied on droplet positioning. This difficulty can be reduced through the use of micromanipulators, microfluidic flows, gravity and electrical fields [17, 18]. The main advantage stems from the ability to automate and parallelize this system [19, 20].

The first attempt at developing a similar high-throughput droplet bilayer platform was capable of producing over 2000 bilayers in two hours [21]; however, the positioning of the electrodes required manual manipulation and drastically lowered the feasibility of automation and large-scale operation.

CHAPTER 3: High Throughput Platform

From the 1960's onward, the platform for creating artificial bilayers has only marginally changed, and in some cases has remained the same, such as the popularity of the painted bilayer method. With traditional methods a few bilayers a day were possible. Now, hundreds and even thousands of bilayers can be created and tested using a multitude of conditions and parameters per day. The exponential increase in artificial bilayer output can be primarily attributed to new technological methods and fabrication techniques.

3. 1 Chip Fabrication

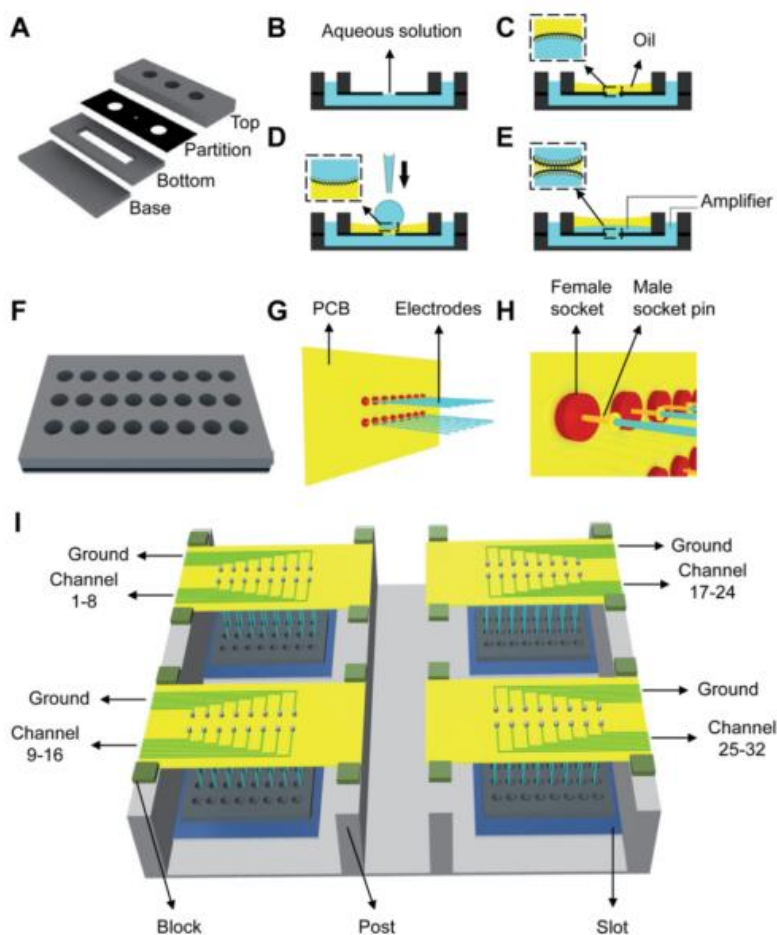


Figure 3. Current platform for bilayer parallelization schematic. [19]

The current platform design has been a work-in-progress for many years and is the basis for experimentation throughout this thesis [22, 23]. The partition is composed of a 75 μ m thick

sheet of Delrin® containing apertures ranging in size from 200-1000µm depending on the conditions of the experiment. The exploded chip view shown in (A) displays the small aperture within the partition layer sandwiched between acrylic plastic layers which create the volumes containing the top and bottom aqueous solutions required for bilayer formation. (B) through (E) show illustrations of the droplet bilayer method which is further described in Appendix A. (F) is an illustration of the completely manufactured bilayer “chip”. (G) and (H) show a simplified illustration of the PCB and electrode configuration used for parallelization of bilayer formation and the interchangeability of the electrodes. Finally, (I) is the entire apparatus schematic and overview of the simultaneous measurement of 32 wells. This work was established previously but many improvements were made to the design and quality of manufacturing which drastically improved the formation and stability of the bilayers during testing and will be discussed shortly.

3. 2 Bilayer Formation

The general method for forming bilayers in this platform consists of the following:

- 1) Add 450uL of an aqueous buffer solution is added to the bottom well.
- 2) Add 10ml of 10mg/ml phospholipid-oil solution.
- 3) Wait 10 minutes for stable bottom monolayer formation.
- 4) Add 50uL of aqueous buffer solution to the top well.
- 5) Wait 10 minutes for stable top monolayer formation.
- 6) Add 50uL of aqueous buffer solution to the bottom well to increase the hydrostatic pressure to begin the process of joining the monolayers to form a bilayer.
- 7) Repeat step 6) until bilayer formation has been achieved.

Modifications to this general process are used for specific lipid compositions and various test conditions as described in a later discussion. This method for bilayer constitution is described in further detail in Appendix A.

Formation of the lipid bilayer membrane is achieved by monitoring the capacitive current of the membrane. A triangle wave voltage of alternating 10mV is applied to establish a charged membrane. The resulting current is measured using a voltage-clamp technique. By establishing the base capacitive current measured before establishing a bilayer and then subsequently after and subtracting the difference, the membrane size can then be mathematically evaluated from the following equations:

$$I = C \frac{dV}{dt} \quad (3.1)$$

$$C = \epsilon_r \epsilon_0 \frac{A}{d} \quad (3.2)$$

Dielectric constant,	$\epsilon_0 = 8.854\text{E-}12 \text{ F} \cdot \text{m}^{-1}$
Relative statistic permittivity,	$\epsilon_r = 2$
Bilayer thickness,	$d = 5\text{nm}$
Bilayer area,	$A = \pi r^2$

By rearranging equation 3.1 to solve for C and then using this value in equation 3.2 to solve for the area, the approximate bilayer area and diameter can be estimated. One drawback of this method is the current measured during the imposed triangle wave can lead to a false positive of bilayer formation. When the monolayers are formed, a capacitive current begins to form; however, the distance between the two monolayers is relatively large compared to that of the bilayer, which is roughly 5nm. As the monolayers begin to join, the capacitive current will grow and when the bilayer is formed, the current generated by the triangle wave input voltage will begin to look flat, which is indicative of capacitive charging and subsequently membrane

formation. Depending on the bilayer lipid composition used during the experiment, and various aspects of the platform, such as aperture size or film thickness, the characteristics of the capacitive current and thus bilayer formation will change.

A guaranteed method for assuring bilayer formation has occurred is referred to as “zapping” the bilayer. This method, simply put, breaks the bilayer by applying a large potential over the bilayer very quickly. If there is a bilayer present, it will break, causing the capacitive current to be shorted and is very obvious in the current readouts in the data acquisition. If a bilayer has yet to form, the capacitive current will remain unchanged. The obvious downside to this method is that it destroys the bilayer, confirming its presence but also concluding the experiment in the process. Although destructive in nature, this method of bilayer confirmation is useful when determining if a small control bilayer is truly a bilayer at the end of a long experiment.

An additional method for verification of membrane formation is the addition of a membrane protein such as gramicidin. This protein will only lower the conductance of the membrane when the thickness is biomolecular, as two proteins, each half the width of a bilayer in thickness, need to come together to form a pore for ions to flow through. By applying a constant voltage across the membrane, a change in current will be observed in the form of a “step” current as the membrane conductance lowers when the pore is formed and ions are permitted to flow through the membrane. When these step currents are observed, bilayer membrane formation is confirmed. This is clearly represented below in Figure 4. The “stepping” of the current is evidence of bilayer formation and the number of steps observed correlates to the number of open ion channels present in the membrane. The size of each individual step correlates to the type of channels used in the membrane, the conductivity of the aqueous solutions surrounding the membrane and the voltage potential applied during the experiment.

These particular proteins can also close, which is observed by the downward step of current of equal value as the open step current. Some protein channels will also allow different amounts of current through depending on which direction the voltage potential is applied. The insertion of membrane proteins has many relevant uses and will be discussed later.

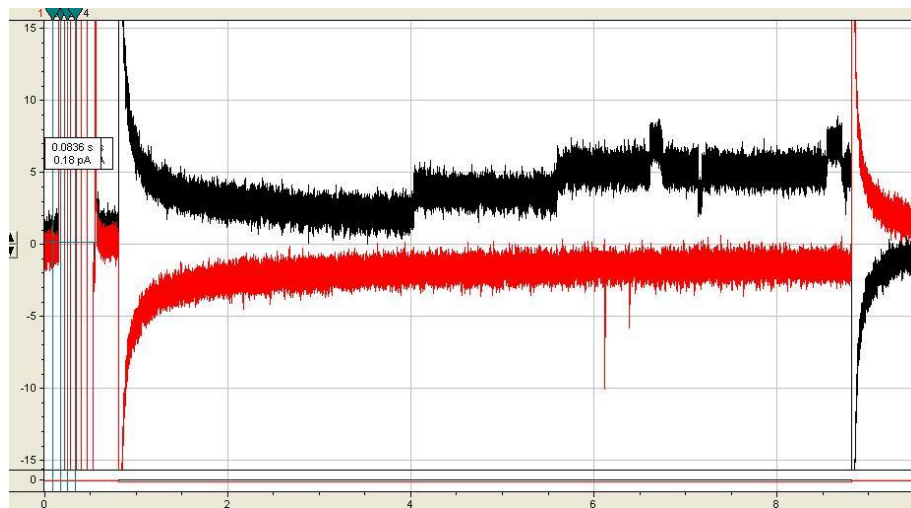


Figure 4. Gramicidin channels confirming bilayer membrane formation.

When first working with bilayer membranes and deducing formation via electrical signals it can be rather daunting at times; however, after understanding the equations mentioned previously and observing the capacitive currents generated from bilayers and non-bilayers, generally speaking, an experienced researcher can confidently assume when a bilayer has formed without the addition of membrane proteins or zapping the bilayer. As previously mentioned, various combinations of lipids and aperture sizes can change the required capacitive current needed to assume a bilayer has formed; however, in the case of using Tecella©, we have yet to observe a lipid composition that is not a bilayer when the capacitive current is at or above 180pA. This has become the standard current level for confirming bilayers using the Tecella© amplifier for the current iteration of bilayer chips.

CHAPTER 4: Technology Innovations

4.1 Laser Characterization

One problem that has plagued the artificial bilayer community for the past half a century has been the longevity and feasibility of the bilayers. In many cases there is a tradeoff between bilayer stability and access to both monolayers. Initially, the current platform could produce stable artificial bilayers with 91% efficiency as observed in the data found in Table 1 shown below using DPhPC (1,2-dioleoyl-sn-glycero-3-phosphocholine) lipid bilayers. A bilayer was considered to be stable if it maintained a capacitive current of 150pA for greater than 30 minutes.

Table 1. Bilayer formation and fusion rates before laser characterization.

Date	Formed	Fused
16-Apr-2013	4	1
17-Apr-2013	4	1
18-Apr-2013	2	0
22-Apr-2013	0	2
23-Apr-2013	3	2
24-Apr-2013	4	0
25-Apr-2013	3	0
26-Apr-2013	3	1
29-Apr-2013	2	0
30-Apr-2013	5	1
9-May-2013	6	0
2-May-2013	7	1
3-May-2013	8	0
6-May-2013	22	2
7-May-2013	12	6
8-May-2013	16	0
9-May-2013	7	1
10-May-2013	16	0
13-May-2013	14	2
14-May-2013	23	1
15-May-2013	23	1
17-May-2013	8	0
22-May-2013	7	1
23-May-2013	14	2
29-May-2013	8	0
30-May-2013	8	0
31-May-2013	13	3
	Formed	Fused
Total:	242	28

After observing the apertures under a 10X microscope and comparing which wells formed good bilayers and which bilayers did not form bilayers or unstable bilayers, there appeared to be a direct correlation between the shape and consistency of the aperture and the bilayer formation rate. The more circular the aperture, the more likely it was to form a good bilayer. An example of what would be considered a poorly formed aperture is shown below in Figure 5.

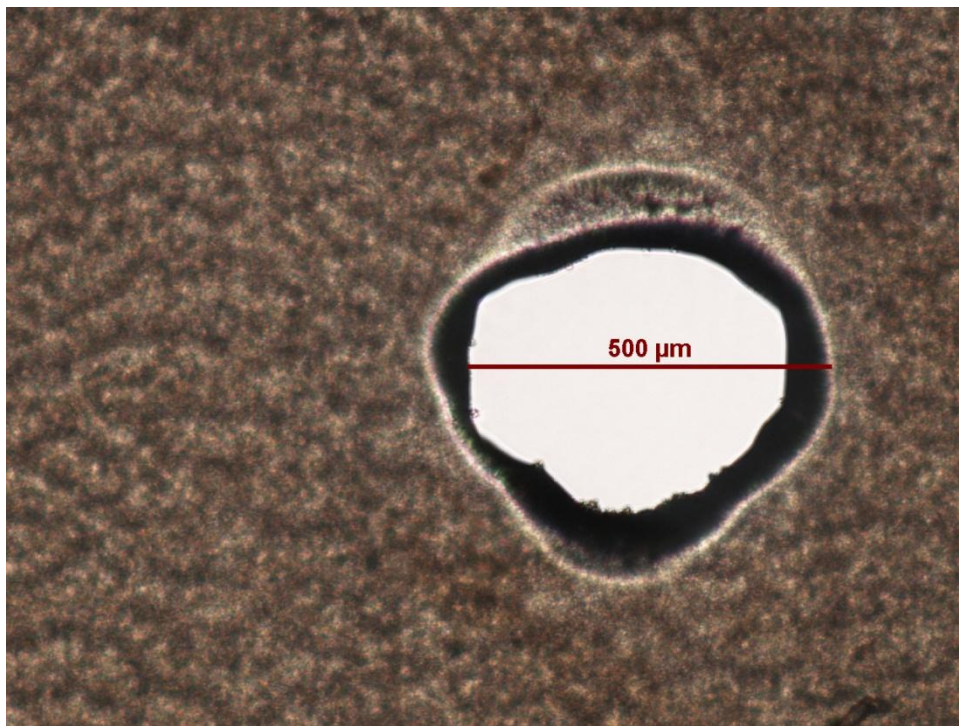


Figure 5. A poorly formed aperture that resulted in an unstable bilayer during a previous experiment is observed under a 10X microscope for characterization.

Although the exact reason for the discrepancy in aperture formation and bilayer yield is not known, there seemed to be a correlation. Further research into the fabrication of the bilayer aperture was needed to resolve this problem.

To begin, the location of the film on the laser cutting board was brought under scrutiny to determine if this was relevant to the circularity of the aperture holes. The upper left quadrant of the laser cutting board is the typical area used for fabrication so this became the area of interest. The Delrin® film used to create the apertures were taped flat onto the laser cutting surface and

the standard parameters of 10% power, 10% speed and 1000 DPI were used over the course of the experiments to maintain consistency. After observing the laser cutter during fabrication, a reflected beam of light could be periodically observed as the laser followed its standard protocol. To the un-aided eye, there was no obvious damage to the film. Under the microscope, it was clear the reflected laser light from the metal mesh support was causing discrepancies in the film apertures as shown below in Figure 6.

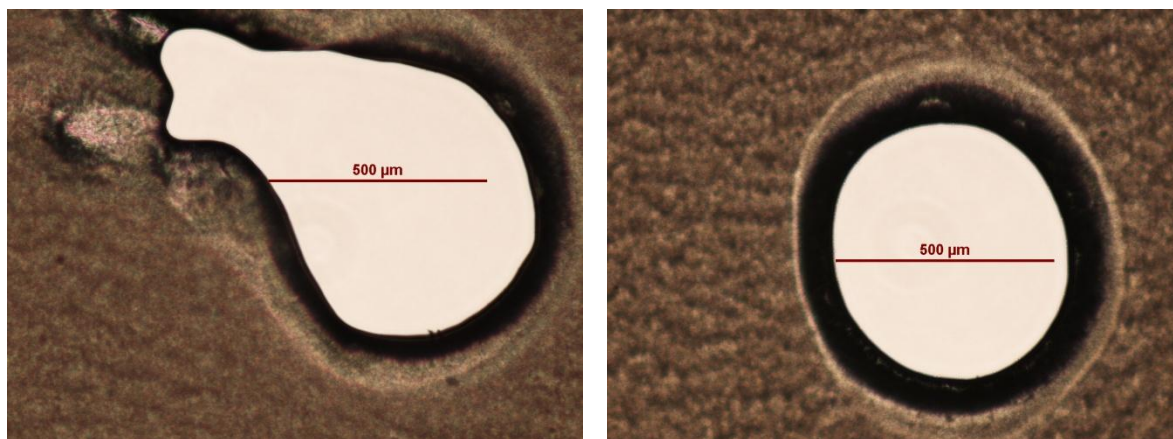


Figure 6. (Left) The juxtaposition of the result of reflected laser on aperture formation and a typical aperture produced by the laser cutter (right).

This experiment was repeated six times with the film used in the upper right quadrant and the same laser protocol used and the results were consistent. The metal support mesh was reflecting light and damaging the same wells on each partition with predictable accuracy. The solution was simple. By elevating the Delrin® film off of the metal support mesh by just a quarter of an inch, inconsistencies in the apertures could be completely eliminated. This was accomplished by using an old acrylic quarter inch template from a previous project, which allowed the laser to cut through the Delrin® film but not cut the acrylic, as shown in Figure 7.

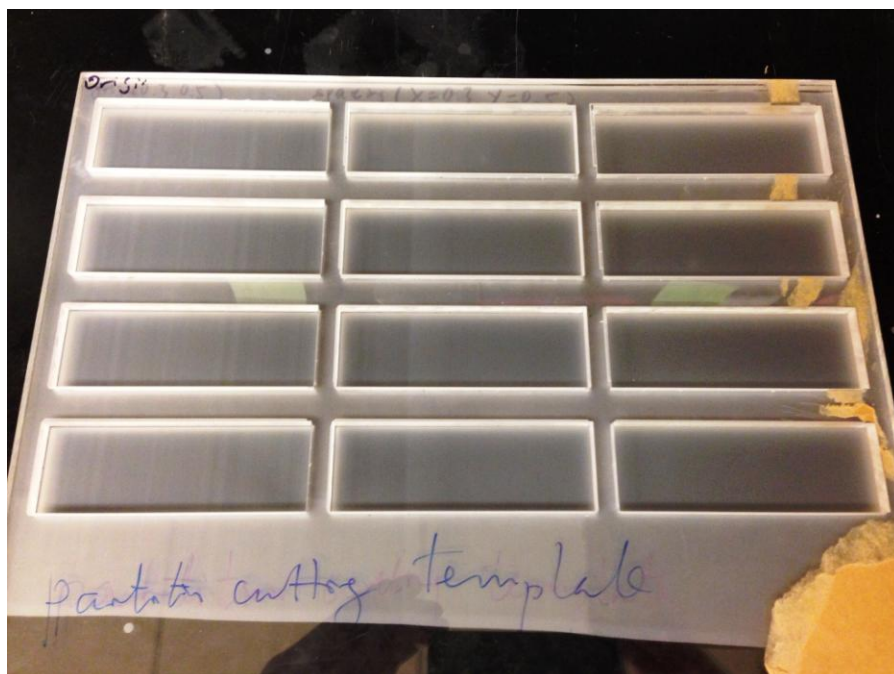


Figure 7. Acrylic film template designed for consistent aperture fabrication. Two quarter-inch acrylic plates sandwich a thin sheet of Delrin® film to elevate and hold the film above the laser cutting board.

This benefited the chip fabrication in two incredible ways. One, this provided confidence in the laser's ability to provide consistent aperture sizes and shapes and second, it removed the need to constantly check the apertures for circularity and diameter consistencies. For the case of large-scale experiments where multiple chips are used per day, this drastically reduces the time needed on quality control and fabrication and allows for more time and effort to be spent on experimentation and data analysis. In a brief subsequent testing of the platform using DPhPC bilayers, the yield was hovering just below 100%, typically with perfect yield or at most 1/24 wells fusing in control experiments.

4.2 Measurement Automation

In addition to fabrication, the quality control aspect of the chip-making process also needed to be improved. Similar to the fabrication process, checking the partitions every time they were fabricated was time consuming and inefficient. Taking the partitions to a microscope and laboriously looking at every aperture to scrutinize its size and shape was not only tedious it was

also very subjective. The traditional method utilized image processing software called ImageJ to manually measure the horizontal diameter of each aperture and outline each aperture by drawing a circle over the estimated circumference of the aperture. By collecting enough measurements to obtain statistically relevant data, a conclusion of whether or not the apertures were consistent or not and could then be used to construct more chips. Although this method worked, it was very inefficient and the measurement was only of the horizontal diameter, and not the average diameter. For a perfect circle this wouldn't matter but because the apertures are more oval-shaped than circular as shown in Figure 8. In this case, it is better to get an average diameter measurement.

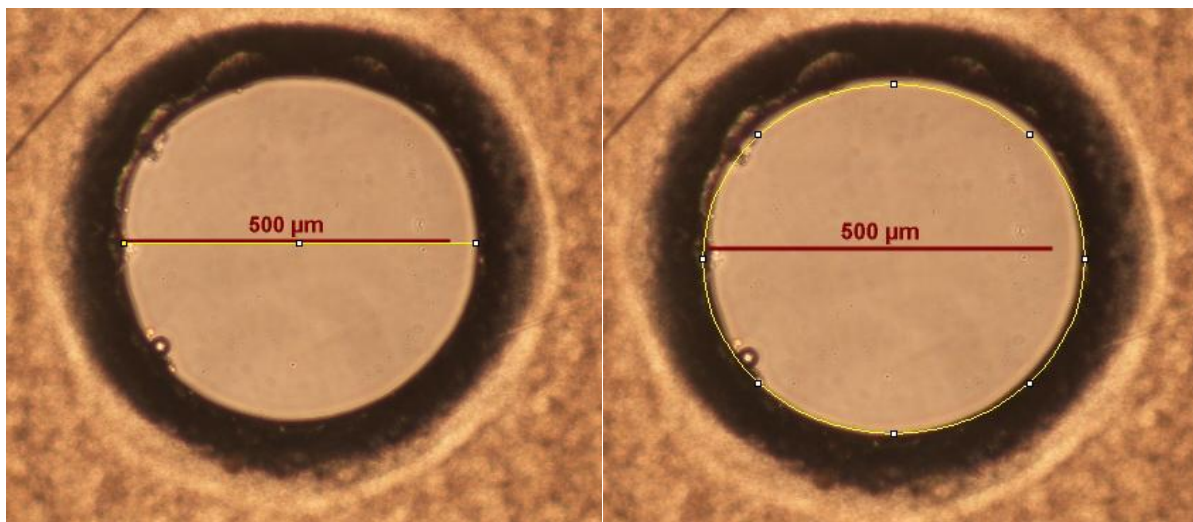
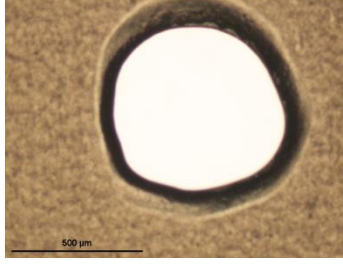
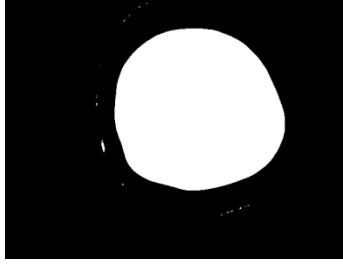
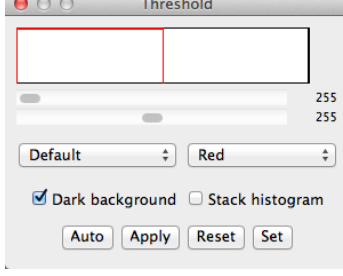
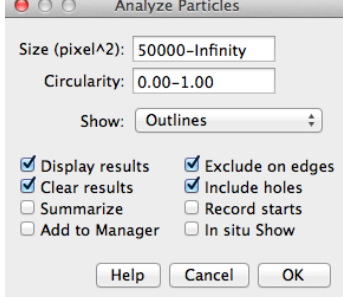
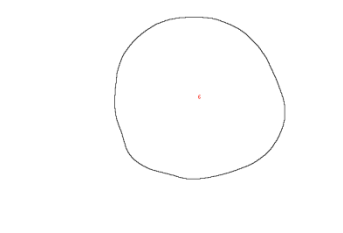


Figure 8. (left) The diameter of the aperture measured by the yellow horizontal line and (right) the area of the aperture measured by the area within the yellow circle in ImageJ.

The subjective aspect and tedious manual measurements inspired a change to the traditional method in support of a more automated and objective measurement of the apertures. The following method in Table 2 was used to take a large sequence of images and export an Excel file with accurate measurements of the aperture diameters and areas:

Table 2. ImageJ aperture quantitative analysis protocol.

	<ol style="list-style-type: none"> 1. File 2. Import 3. Image Sequences <ol style="list-style-type: none"> a. Select the folder containing the apertures for measurement 4. Click “OK” <p>A window will pop up displaying a side-scroll of all the images collected from the folder.</p>																																																																																																
	<ol style="list-style-type: none"> 5. Process 6. Binary 7. Make Binary <ol style="list-style-type: none"> a. Select the check box to “Calculate threshold for each image” 8. Click “OK” <p>The images have now all been converted to black and white. Note: as shown in the image to the left, there will be small white artifacts in the image but they will be filtered out later.</p>																																																																																																
	<ol style="list-style-type: none"> 9. Image 10. Adjust 11. Threshold <ol style="list-style-type: none"> a. The window to the left will now be visible 12. On the left drop-down menu, select “Default” as shown. If it is selected, select it again for the slide bars to automatically adjust. 13. Click “Apply” 																																																																																																
	<ol style="list-style-type: none"> 14. Analyze 15. Analyze Particles <ol style="list-style-type: none"> a. Set the minimum size to 50,000 and the maximum to infinite b. In the Show drop-down, select “Outlines” c. Check the four boxes shown on the left 16. Click “OK” 																																																																																																
	<p>A window will appear with the outlines of each aperture to visually verify each well was outlined properly. Compare this to the original images (a few) to check for consistency.</p>																																																																																																
<table border="1" data-bbox="186 1732 527 1892"> <thead> <tr> <th></th> <th>Area</th> <th>Perim.</th> <th>Feret</th> <th>FeretX</th> <th>FeretY</th> <th>FeretAngle</th> <th>MinFeret</th> </tr> </thead> <tbody> <tr><td>1</td><td>70740</td><td>1001.5</td><td>314.0</td><td>202</td><td>103</td><td>136.3</td><td>289.6</td></tr> <tr><td>2</td><td>72834</td><td>1017.4</td><td>319.1</td><td>228</td><td>137</td><td>141.9</td><td>290.9</td></tr> <tr><td>3</td><td>75770</td><td>1110.2</td><td>330.2</td><td>181</td><td>181</td><td>151.4</td><td>307.3</td></tr> <tr><td>4</td><td>75760</td><td>1037.3</td><td>326.1</td><td>209</td><td>148</td><td>150.2</td><td>303.2</td></tr> <tr><td>5</td><td>75198</td><td>1034.0</td><td>326.6</td><td>216</td><td>146</td><td>150.1</td><td>300.7</td></tr> <tr><td>6</td><td>74502</td><td>1026.6</td><td>325.1</td><td>220</td><td>123</td><td>150.5</td><td>298</td></tr> <tr><td>7</td><td>73140</td><td>1019.6</td><td>320.8</td><td>171</td><td>163</td><td>144.1</td><td>293.9</td></tr> <tr><td>8</td><td>72838</td><td>1019.2</td><td>318.4</td><td>243</td><td>143</td><td>143.8</td><td>291.8</td></tr> <tr><td>9</td><td>76950</td><td>1041.8</td><td>324.1</td><td>231</td><td>132</td><td>149.4</td><td>301.6</td></tr> <tr><td>10</td><td>75988</td><td>1039.2</td><td>322.8</td><td>222</td><td>164</td><td>150.9</td><td>296.2</td></tr> <tr><td>11</td><td>78832</td><td>1054.2</td><td>328.6</td><td>361</td><td>78</td><td>95.6</td><td>301.3</td></tr> </tbody> </table>		Area	Perim.	Feret	FeretX	FeretY	FeretAngle	MinFeret	1	70740	1001.5	314.0	202	103	136.3	289.6	2	72834	1017.4	319.1	228	137	141.9	290.9	3	75770	1110.2	330.2	181	181	151.4	307.3	4	75760	1037.3	326.1	209	148	150.2	303.2	5	75198	1034.0	326.6	216	146	150.1	300.7	6	74502	1026.6	325.1	220	123	150.5	298	7	73140	1019.6	320.8	171	163	144.1	293.9	8	72838	1019.2	318.4	243	143	143.8	291.8	9	76950	1041.8	324.1	231	132	149.4	301.6	10	75988	1039.2	322.8	222	164	150.9	296.2	11	78832	1054.2	328.6	361	78	95.6	301.3	<p>An Excel sheet will also be simultaneously generated with the area, perimeter and various diameter measurements listed.</p>
	Area	Perim.	Feret	FeretX	FeretY	FeretAngle	MinFeret																																																																																										
1	70740	1001.5	314.0	202	103	136.3	289.6																																																																																										
2	72834	1017.4	319.1	228	137	141.9	290.9																																																																																										
3	75770	1110.2	330.2	181	181	151.4	307.3																																																																																										
4	75760	1037.3	326.1	209	148	150.2	303.2																																																																																										
5	75198	1034.0	326.6	216	146	150.1	300.7																																																																																										
6	74502	1026.6	325.1	220	123	150.5	298																																																																																										
7	73140	1019.6	320.8	171	163	144.1	293.9																																																																																										
8	72838	1019.2	318.4	243	143	143.8	291.8																																																																																										
9	76950	1041.8	324.1	231	132	149.4	301.6																																																																																										
10	75988	1039.2	322.8	222	164	150.9	296.2																																																																																										
11	78832	1054.2	328.6	361	78	95.6	301.3																																																																																										

Within the Excel document, there is a term labeled “Feret” which is analogous to a maximum diameter. The Feret diameter, also known as the caliper diameter is defined by Gregorova as the, “normal distance between two parallel tangent planes touching the particle outline” [24, 25]. This implies a dependence on orientation and ImageJ takes this into consideration by rotating each particle a set number of times depending on the internally programmed parameters to come up with a maximum diameter of the particle, or Feret diameter. This same procedure is used to determine the minimum Feret diameter. The ratio between the maximum and minimum Feret diameter is known as the aspect ratio. For a perfect circle, the aspect ratio is one. Ideally, the apertures would be as circular as possible, i.e. with an aspect ratio as close to one as possible to maintain consistency when running experiments. These parameters are ideal for objectively determining the characteristics of the apertures and are quickly and easily found using the ImageJ software protocol mentioned previously in Table 2. Although these changes to the procedure were small, they greatly affected the output of the experiments by controlling a previously unknown variable of the bilayer array platform, thus resulting in a higher consistency of formed and stable bilayers. More importantly, by knowing the apertures were being fabricated consistently and to the specifications we were looking for, it was established ahead of time that bilayer failure would rarely, if ever, be the result of poor aperture fabrication and could be attributed to other variables within the experiment.

Chapter 5: Current Applications

As science has progressed, the need to understand smaller and smaller biological processes to understand the greater picture has become evident. The term nanotechnology has become synonymous with next-generation medicine and has found a suitable use in our platform via what are commonly referred to as nanoparticles. A nanoparticle is any microscopic particle with at least one dimension less than or equal to 100nm. Nanoparticles have recently been shown to have an amazing potential as a means of detection and diagnostic tool in medical applications[26]. Through parallelization and high through-put techniques described in this chapter, the relationship between nanoparticles and detection and diagnostic abilities is investigated.

The current state of this platform has transitioned from that of synthetic phospholipids, such as DPhPC in combination with protein pores such as α -Hemolysin and Gramicidin to more natural compositions that represent the plasma membrane and intra-cellular organelles. This transition was made to better simulate cellular conditions and bring lab-conditioned artificial membranes closer to mimicking their cellular counterparts. In addition to the change in lipid composition, there has also been a strong emphasis towards investigating the effect of nanoparticles on these membrane systems.

The first venture into nanoparticles started with the highly-studied amine-modified polystyrene nanoparticles. Wang's group reported that these amine-modified polystyrene nanoparticles induced cell death by accumulating in the lysosomes leading to the release of cathepsins (proteases) which ultimately degrade the mitochondria and subsequently resulting in cell death [27]. In this particular study, cell cultures were used with various inhibitors of cellular pathways to diagnose the mechanisms of cell death. These results and others offer a great opportunity to look at the various cellular mechanisms and effect of nanoparticles on real

biological systems; however, as stated by the author, “the details of the mechanism by which these positively charged particles induce such damage to the lysosomes still remain unresolved”. Alas, our platform has the opportunity to help lift the veil of uncertainty and quantitatively decipher the mystery surrounding the interaction between these nanoparticles and lysosomal membranes through the ability to collect large amounts of data via parallel arrays of experiments.

Earlier techniques at creating membranes in parallel used simple synthetic phospholipids such as the neutral lipid DPhPC or a combination of POPC (1-palmitoyl-2-oleoyl-*sn*-glycero-3-phosphocholine) and POPE (1-palmitoyl-2-oleoyl-*sn*-glycero-3-phosphoethanolamine) to create simple membranes. These membranes were initially used to cross-examine our observations with nanoparticles with previous studies utilizing studies based on cell responses. The first experiment used pure POPE bilayers to establish a baseline for interaction and bilayer stability as shown in Table 3.

Table 3. A summary of the nanoparticle interaction data with pure POPE lipid membranes.

Experimental Summary: POPE Bilayers (pH 7.0)				
Particle	Concentration	Ionic Strength	Interaction/Fusion (total bilayers tested)	Time To Interaction (min)
NH2-PS	25ug/ml	80mM	2/1 (5)	163, 149
COOH-PS	25ug/ml	80mM	2/3 (4)	36, 25
--	Control	80mM	2/1 (6)	--
NH2-PS	25ug/ml	150mM	2/0 (5)	149, 162
COOH-PS	25ug/ml	150mM	4/2 (4)	38, 69, 149, 149
NH2-PS	100ug/ml	150mM	1/4 (4)	2
COOH-PS	100ug/ml	150mM	2/0 (4)	8, 37
--	Control	150mM	2/0 (4)	--
COOH-PS	25ug/ml	5mM	0/2 (6)	--
NH2-PS	25ug/ml	5mM	0/4 (4)	--
--	Control	5mM	0/0 (5)	--

At first glance, it would appear that there is a significant interaction from both the amine-modified and carboxyl-modified nanoparticles; however, it is important to state that although the controls are considered to be good wells, a large portion of wells in each of the above

experiments fused before any nanoparticles were added to solution. This particular lipid composition was very difficult to work with because the bilayers were generally difficult to form and were very sensitive to the bottom well volume. Despite the low bilayer yield, the effect of ionic strength on the interaction and fusion rates of amine-modified particles can be observed.

To better understand what is meant by interaction and fusion it is important to discuss the various types and what it means for a nanoparticle to interact with a bilayer, electrically speaking. It is important to distinguish what is meant by an “interaction” and the relevance to what a fusion or interaction would mean in terms of a biological mechanism.

5.1 Nanoparticle Interaction

The simplest observable form of interaction is when a bilayer spontaneously fuses. The term “fuse” refers to the two aqueous phases fusing together to allow a large flux of current between the two chambers creating a current which is easily observed using the Tecella© amplification software, as observed in Figure 9.

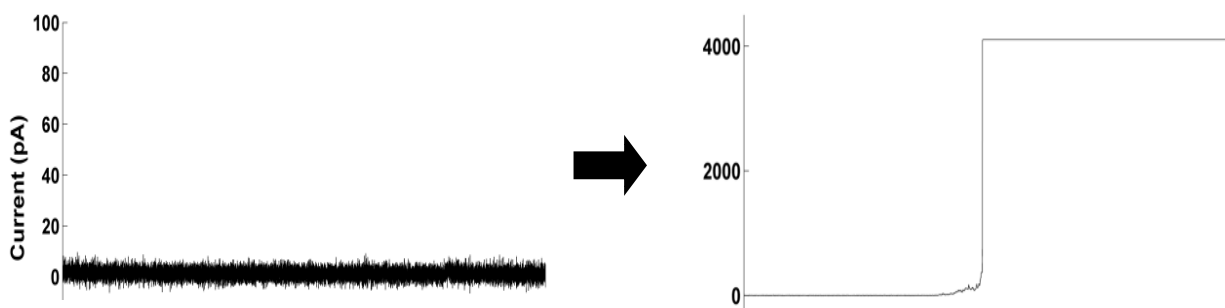


Figure 9. A simplified view of a large influx of current as a result of an immediate bilayer fusion. (Left) a flat current reading centered at 0pA without any noise or leak currents observed. (Right) A fusion event observed by an influx of current and plateauing at the maximum current reading of 4000pA.

Unfortunately, the simplicity of a spontaneous fusion also tells us very little about the biological mechanism. In this case, it is only apparent that the nanoparticle in question interacts with the bilayer very quickly and would likely cause cell death. As the membrane lipid

composition is altered, the mechanism of nanoparticle interaction can be further investigated under conditions more analogous to reality. In many cases, by lowering the concentration of the nanoparticles a more prolonged interaction will take place and further analysis can be performed to understand the mechanism of interaction.

More specifically, by lowering the concentration of nanoparticles, the interactions may become more drawn-out or even transient. It has been hypothesized that the sharp fluctuations in current are evidence of perforations in the membrane and subsequent reformation of the membrane when the current returns to baseline, as shown in Figure 10.

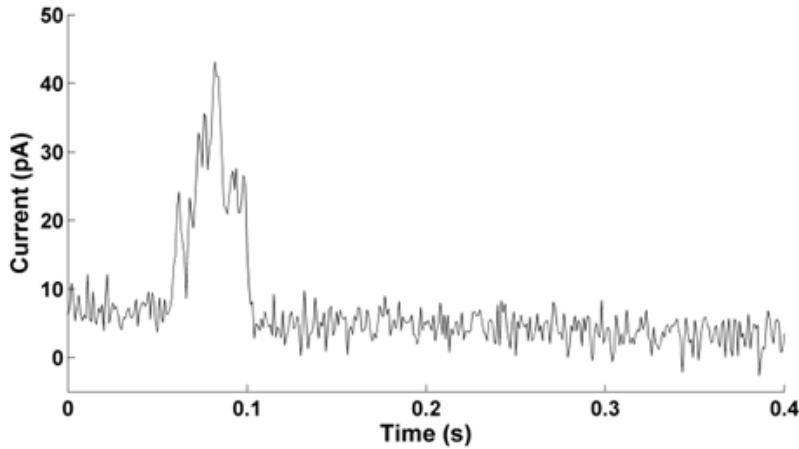


Figure 10. An example of a nanoparticle interaction event where a transient pore formation and subsequent reformation of a stable bilayer membrane takes place.

The size of these current steps can be grouped by histogramming the various jumps in current over a given data set and then the average pore size can be mathematically estimated using the following formulas:

Conductance (G):
$$G = \sigma \frac{\pi r^2}{l} \tag{5.1}$$

Pore length (l):
$$l = 5E - 9m \text{ (bilayer thickness)}$$

Electrical conductivity:
$$\sigma = 9.2E-2 \text{ S/m @80mM NaCl}$$

Equation 5.1 relates conductivity to the square of the radius of the pore. The conductivity (G) is the inverse of the change in resistance of the membrane. This change in resistance is noted by an influx of current through the membrane as a result of the pore formation. The well-known equation $V = I * R$ comes into play here to find the relationship between the current reading and conductance of the membrane. If we take into consideration the inverse relationship between conductance and resistance, the equation then becomes, $G = \frac{I}{V}$. The voltage alternates between positive and negative 70mV in roughly 30 second intervals. An example of the current reading and mathematical calculation is displayed with the following data from Figure 12.

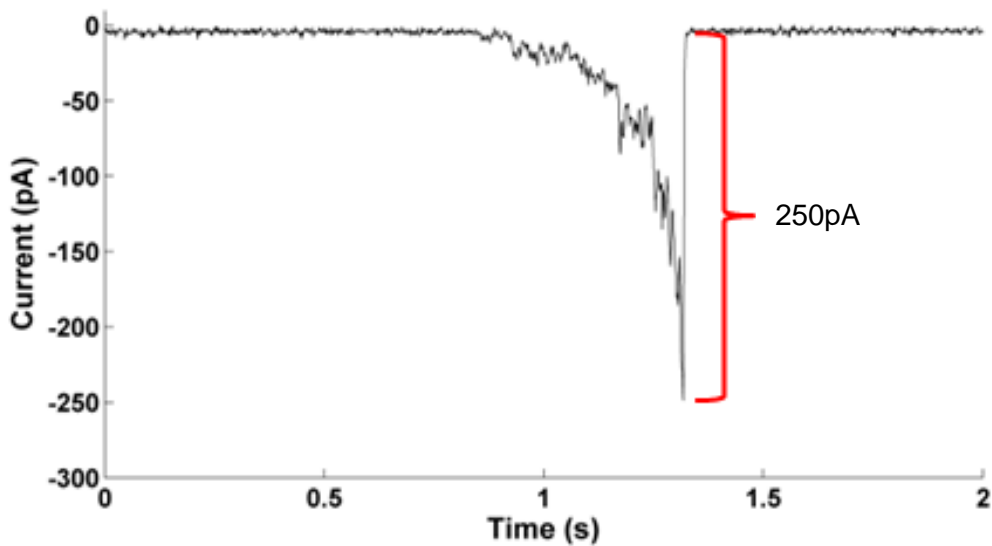


Figure 11. An example of the current used to quantify the transient pore size in a membrane.

By using the 250pA found in Figure 12 and knowing the voltage applied during this sweep was -70mV, the conductance can be concluded to be 3,570nS. The only unknown variable is the radius which can be quickly calculated using equation 5.1 to be ~2.3nm. The pore size calculated in this example is very small compared to the amine-modified polystyrene nanoparticles used in these experiments, which are on the order of about 30nm in diameter. This brings up an interesting result because this would seem to insinuate that the nanoparticles are not

pushing themselves through the pore, but are possibly removing lipids from the membrane which might explain why the pore radii are so small. Further research into pore formation is needed to accurately conclude how these pores are formed.

Although it is difficult to conclude the exact interaction between the nanoparticles and the artificial membranes, steps have been made toward this goal. In addition to looking at the various types of interactions present during the experiment and pore formation, it is also very important to look at when the interaction takes place. Each voltage protocol includes a lengthy portion of a positive 70mV voltage sweep of about 30 seconds followed by an equivalently long duration of a negative 70mV voltage sweep. By performing a large number of experiments under the same biologically mimicked conditions and concentration of nanoparticles, we can discern if the nanoparticles have a bias towards interaction or fusion during either of these voltage sweeps, if at all. The electrodes on the platform are always placed in the wells such that the ground electrode is connected to the bottom well and the active electrode is placed in the top well. The nanoparticles are always put in the top well. Diffusion and influences from the induced electrical field move the nanoparticles toward/away from the bilayer depending on the charge of the particle used as well as whether or not the voltage sweep is currently positive or negative. The following example in Figure 13 displays the observed effect of voltage dependence on bilayer interaction for amine-modified nanoparticles using the Tecella© multi-channel amplifier and protocol found in Appendix A.

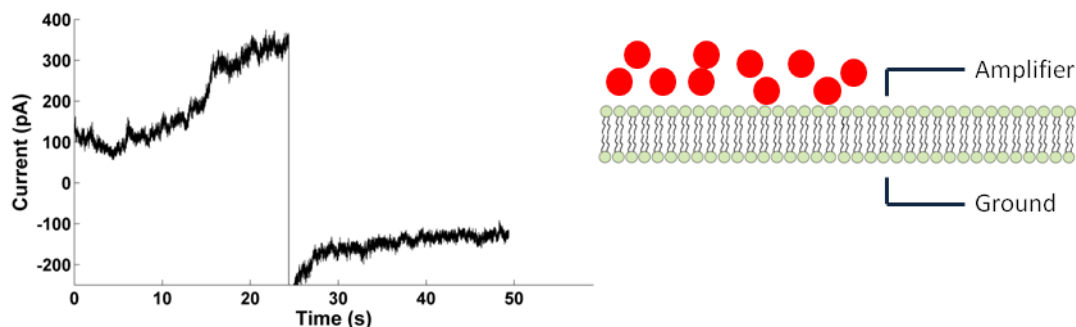


Figure 12. (Left) Amine-modified nanoparticles interacting with a consistent dependence on the sign of the voltage sweep. The amine-modified nanoparticles consistently interact during the positive voltage sweep. (Right) An illustration of the location of nanoparticles relative to the electrode placement.

5.2 Artificial Physiological Membrane Compositions

As mentioned previously, membranes are complex and difficult to reproduce on a large scale. Cell studies are a fantastic way to use real biological systems to accurately mimic real-life scenarios and conditions; however, when looking deeper into the cell, it is very difficult to effectively study the intracellular membranes such as the lysosomal or mitochondrial membranes. By altering the lipid composition of the membranes, the plasma membrane and various intracellular membranes can be accurately established *in vitro*. Experiments like the one conducted on the pure POPE membranes as well as other lipids, such as POPC, combinations of POPC, POPE and cholesterol (Chol), and including lipids like Cerebroside (CB) and Phosphatidylserine (PS), these incredibly stable and biologically relevant membranes were established.

Prior to determining these lipid compositions, brain (porcine) and heart (porcine) extracted lipids were experimentally used as they were useful as a potential benchmark for future biologically relevant lipid combinations. In general, the brain and heart extracts are predominantly composed of PE, PC and PS lipids. There are additional lipids found in these total extracts; however, for our purpose, the previously listed lipids are a good starting point for building our own model for representing biologically relevant membranes.

Initially, the total brain extract lipid composition was used to test amine-modified and carboxyl-modified nanoparticles. Ekkapongpisit et al. found the carboxyl-modified nanoparticles to be non-toxic for concentrations up to 75ug/ml [28]. Larger concentrations were not tested but a range of particle sizes were tested that were on the same order of magnitude as the particles used in our experiments so this was a good benchmark to compare our data with. Ekkapongpisit also found the amine-modified nanoparticles to be highly cytotoxic, particularly at larger particle sizes. The range of tested particles was 30-50nm for carboxyl-modified and 50-1000nm for amine-modified nanoparticles. Interestingly, the cell compartmentalization of these nanoparticles was determined to be located within the lysosomes. From this data we were able to begin testing various conditions to begin to simulate these results within our artificial membranes. In Table 4, the first round of nanoparticle data was collected using the total brain extract lipid under physiologically relevant conditions of pH 7.0 and 150mM NaCl.

Table 4. Total brain lipid extract bilayers under plasma membrane conditions were tested using carboxyl and amine-modified polystyrene nanoparticles. *Noise currents associated likely from an unclean chip.

Total Brain Extract Bilayer Results Summary (pH 7 & 150mM NaCl)				
Particle/Condition	Concentration	Total Wells Tested	Interactions	Fusion
NH ₂	100ug/ml	24	1	24
COOH	100ug/ml	8	2	1
Control	0ug/ml	8	1*	0
Serum +10% FBS Control	0ug/ml Control	24	6	22
Serum +10%FBS NH ₂	100ug/ml	7	1	7

In this first data set, it is apparent that the amine-modified nanoparticles at a concentration of 100ug/ml are toxic to this particular lipid composition in physiologically relevant conditions. In addition, only one of the eight wells tested with carboxyl-modified nanoparticles fused which is insignificant when considering that under the same conditions, twenty-four out of twenty-four amine-modified nanoparticle experimental wells fused. The

control group also showed similar results to the carboxyl-modified nanoparticle conditions. The question then arises as to whether the experiment was long enough to detect an interaction with the carboxyl-modified nanoparticles. Unfortunately, it is difficult to prolong these experiments due to the nature of the stability of these bilayers. It is generally accepted in this platform that an experimental duration for a bilayer to be stable is roughly two hours after adding nanoparticles. After this point, it has been noted that bilayers begin to leak and become unstable, adding variability and uncertainty to the data collected. If the carboxyl-modified particles were interacting with the membranes, it was not able to be detected during the two-hour timeframe given by the experimental protocols.

The 100ug/ml experimental condition was considered to be a fairly high starting point and was used as a yes/no test to determine if these particles were interacting at all with the bilayers. The final two rows of Table 4 offer an interesting conclusion as almost every well in both the control and the experimental groups fused which was not the case in the previous experiments. The condition of Serum+10% Fetal Bovine Serum (FBS) was used because this more closely matches physiologically relevant aqueous solutions. This particular solution not only has the correct ionic strength and pH but also has a large diversity of proteins that would be commonly found within the cellular environment. Further testing would conclude that the serum+10% FBS solution would make bilayers unstable and difficult to form; thus, this condition was abandoned because it was not feasible for parallelization at this stage in platform development. The control groups for the non-serum+10% FBS groups were very stable and consistent from experiment-to-experiment. Overall, the results were similar to the findings of Ekkapongpisit and other groups. Although similar findings were concluded, the total brain extract bilayers were difficult to form. More specifically, additional steps were needed to add to the protocol to add more solution to the bottom well to increase the hydrostatic pressure to bring

the monolayers together. In many cases the protocol was different from well-to-well and thus made parallelization difficult because the wells would need to be tended to individually and would also fuse very easily if the hydrostatic pressure became too great from the additional solution. Attempts were made at changing the partition parameters and other factors to increase the bilayer formation yield but to no avail.

It is important to note the power of the platform to quickly and reliably acquire large amounts of data and to quickly conclude experiments and allow the power of statistics to find trends and deduce possible biological mechanisms of interaction. The bilayer stability is heavily affected by the surrounding conditions as well as the lipids present which ultimately compose the bilayers. As the platform has shown near-perfect bilayer yields with DPhPC, it was a matter of altering the lipid composition to bring the bilayer yield to a higher standard for future high-throughput applications.

Moving forward, the total heart lipid extract was tested under similar conditions to check the consistency of interactions across a slightly different lipid composition as observed in Table 5.

Table 5. Total heart lipid extract bilayers under plasma membrane conditions were tested using amine-modified polystyrene nanoparticles.

Total Heart Extract Bilayer Results Summary (pH 7 & 150mM NaCl)				
Particle/Condition	Concentration	Total Wells Tested	Interactions	Fusion
NH2	100ug/ml	5	1	4
Control	0ug/ml	4	0	0

The sample size for total heart extract lipid bilayers is small because, like the brain extract membranes, these bilayers were very small, unstable and difficult in general to form. Although it is obvious from table 5 that the amine-modified nanoparticles interact with the membrane to some degree, it is also important to note that the remaining seven of the sixteen

wells fused before the control or experimental conditions were established. If almost half of the total wells fuse before adding any nanoparticles, the potential for parallelization is extremely diminished. Despite the low yield of bilayer formation, the results were still consistent with the literature. Further investigation of different bilayer lipid compositions was needed to establish a suitable model for the plasma and lysosomal membranes.

After gathering data with preliminary POPE, heart and brain lipid extract bilayers, the search for a reliable, stable and easy-to-use lipid combination began. To begin, pure POPE bilayers were tested under various ionic strengths and particle conditions to further test the viability of POPE as a major component to the final lipid composition, as described in Table 6.

Table 6. POPE lipid bilayers tested under various ionic strengths and concentrations of amine-modified and carboxyl-modified nanoparticles. *Noise currents associated likely from an unclean chip.

POPE Lipid Bilayer Results Summary (pH 7)					
Particle/Condition	Concentration	Ionic Strength	Total Wells Tested	Interactions	Fusion
NH2	25ug/ml	80mM	5	2	1
COOH	25ug/ml	80mM	4	2	3
NH2	25ug/ml	150mM	5	2	0
COOH	25ug/ml	150mM	4	4	2
NH2	100ug/ml	150mM	4	1	4
COOH	100ug/ml	150mM	4	2	0
COOH	25ug/ml	5mM	6	0	2
NH2	25ug/ml	5mM	4	0	4
Control	0ug/ml	5mM	17	0	5

The sample size for these tests are small because, like the extract lipid membranes, pure POPE bilayers are difficult to form and are generally unstable as proven earlier under less variable conditions. This test was repeated to see if varying conditions in conjunction with pure POPE bilayers would have an effect on the bilayer yield. As a pure POPE bilayer, it was difficult under any physiologically relevant ionic strength to form high yielding bilayers. Typically, about a third to a half of all the membranes would either not form or would fuse before adding particles which adds a significant amount of doubt to the remaining membranes during the

experiment. Although POPE is a very common lipid within cellular membranes, it is the balance of other lipids such as POPC and others that make POPE a viable component in artificial membranes. One key point to be made from this data is the affect of ionic strength during the experiments with amine-modified nanoparticles. As the ionic strength increases, the concentration of nanoparticles needed to induce a fusion drastically increases. At this point in data collection it was difficult to characterize the possible interaction events because the number of datapoints from each experiment was small. A more stable lipid composition was needed to better understand the mechanism of nanoparticle interaction. Despite the lower than expected bilayer yield, the fact that pure POPE bilayers could be formed was a good start.

Continuing, a small study on bilayer stability was used as a method to increase the bilayer formation yield which would give us more confidence in our platform and data collection capabilities. By combining POPE and POPC the membranes would be more physiologically relevant and likely more stable. By altering the molar ratios, we could adjust the characteristics of the bilayers and create more stability to increase the overall yield. A study of membrane lipid compositions by Van Meer et al. found the most prevalent lipids within the plasma membrane to also include cholesterol (CHOL) and a negatively charged lipid, POPS [29]. By adding small molar concentrations of these additional membrane components we were able to finally achieve a membrane composition which was physiologically relevant, easy to form, and incredibly stable, in some cases lasting as long as six hours in preliminary test control experiments.

At this point, the high-throughput aspect of our platform was beginning to come together. The characterization of the chips apertures in conjunction with the incredible durability and high-yield of the new bilayer lipid compositions made way for experiments with large impacts on nanoparticle characterization studies. From our preliminary studies, it appeared that ionic strength would be a strong factor in the nature nanoparticle interactions. The decreased number

of fusions and bilayer interactions observed at higher ionic strengths was the first clue of an electrostatic interaction mechanism as observed in Figure 14.

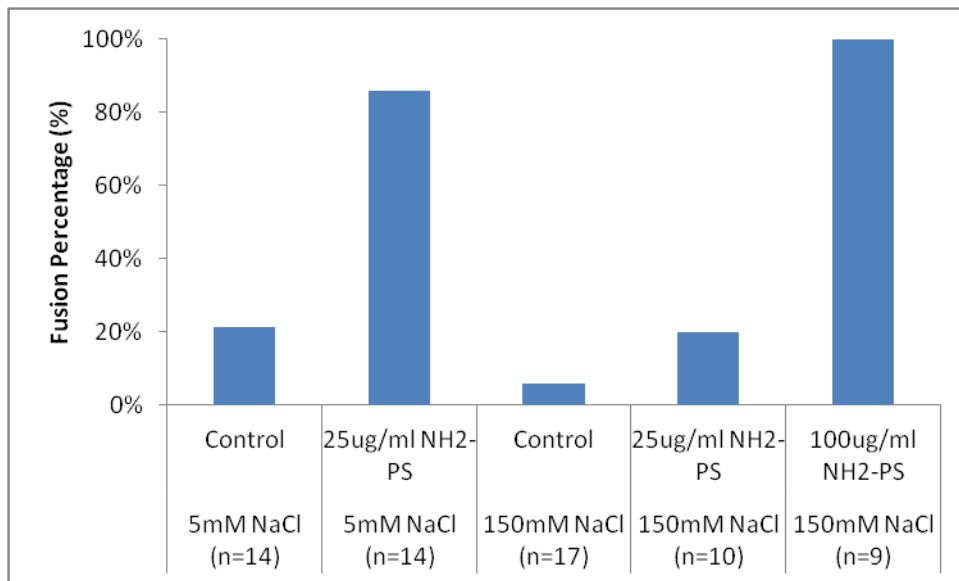


Figure 13. Bilayer fusion rate dependence on nanoparticle concentration and ionic strength.

With a stable combination of lipids determined, the Serum+10% FBS was brought back into experimentation to try to bring the platform even closer to physiological conditions. Table 7 represents the data and commentary found during this experiment in which the stability of these bilayers was found to still be poor; however, the control groups utilizing a 150mM NaCl, 4mM Hepes and pH 7.0 buffers were perfect, in that they did not exhibit any fusions over the two hour experimental duration, a clear improvement.

Table 7. Preliminary data comparing bilayer stability with two different buffer solutions and amine-modified nanoparticles.

December 2, 2013 POPC, POPE, CHOL, POPS 100ug/ml NH2 150mM NaCl pH 7.0; Serum +10% FBS Duration: 120 minutes (2 hours)						
Conclusion: There is a big difference observed in the 150mM wells; however, there is no real difference noted in the Serum wells. Relatively small sample sizes and a few fused before adding NP's. This experiment is repeated on December 3, 2013 with more conclusive results.						
Conditions	Particle	Wells Tested	Interaction	Fused	Comments	Time to fusion (min)
POPC, POPE, CHOL, POPS 150mM NaCl pH 7.0	100ug/ml NH2	5	1/5	5/5	All the wells showed small currents just before fusing but they were not sustained.	6,12,12,12,15
POPC, POPE, CHOL, POPS 150mM NaCl pH 7.0	Control	4	2/4	0/4		---
POPC, POPE, CHOL, POPS Serum +10% FBS	100ug/ml NH2	5	3/5	3/5		84,96,108
POPC, POPE, CHOL, POPS Serum + 10% FBS	Control	5	3/5	5/5	Difficult to form stable bilayers	1,84,85,118,126

In Table 7 it is important to note the time to fusions column. The first row of data shows the experimental group with 100ug/ml amine-modified nanoparticles all fused within the first fifteen minutes after adding nanoparticles to the experimental wells. Without any control groups, this data would be meaningless. The second row is the control group without any nanoparticles added and in this group there were no fusions for the entire two-hour duration of the experiment. This difference alone is enough to conclude a strong interaction between this group of nanoparticles and plasma membranes under physiologically relevant conditions. As stated earlier, this information has already been observed and is not novel but a great proof of concept for our platforms ability to examine many samples in parallel and under conditions that simulate

real conditions. The next test for our platform at this stage was a sense of repeatability and consistency from batch-to-batch of experiments. Table 8 represents a repeated experiment the following day utilizing the same conditions and with very similar results, concluding that our platform offers a consistently high bilayer yield and results that are consistent and repeatable as well as similar to the results found by other groups.

Table 8. Preliminary data illustrating the consistency and repeatability of data collection and test conditions.

December 3, 2013 POPC, POPE, CHOL, POPS 100ug/ml NH2 150mM NaCl pH 7.0; Serum +10% FBS Duration: 120 minutes (2 hours)						
Conclusion: There is a big difference observed in the 150mM wells; however, there is no real difference noted in the Serum wells.						
Conditions	Particle	Wells Tested	Interaction	Fused	Comments	Time to fusion (min)
POPC, POPE, CHOL, POPS 150mM NaCl pH 7.0	100ug/ml NH2	4	0/4	4/4	Same fusion times as the experiment before on December 2,2013	6,6,11,12
POPC, POPE, CHOL, POPS 150mM NaCl pH 7.0	Control	4	2/4	1/4		37
POPC, POPE, CHOL, POPS Serum +10% FBS	100ug/ml NH2	4	2/4	3/4		26,37,51,78
POPC, POPE, CHOL, POPS Serum + 10% FBS	Control	3	2/4	3/3	Fused at the same rate as those with NP's (serum only)	26,52,58

In addition to performing studies on the effect of ionic strength, we also wanted to look at the effect of pH on interaction events and fusion rates. The amine-modified nanoparticles are positively charged while the carboxyl-modified nanoparticles are negatively charged. By adjusting the pH, the amount of available surface charges on the nanoparticles could be altered

and the effect of interaction could be further investigated. The Henderson-Hasselbalch equation was used to describe the effect of pH on the available surface charge of the nanoparticles based on their natural pKa values. By increasing the pH of the aqueous solutions surrounding the membranes, the amine-modified nanoparticles would have a lower surface charge than if the pH were lower. If the interaction between the nanoparticles and the membrane is found to be electrostatic in nature, the nanoparticles with a higher charge density would elicit a more pronounced interaction.

The next experimental variable tested was pH. The amine-modified nanoparticles were tested at a pH of 7, 9.7, 11 and 12 with statistically relevant results confirming the hypothesis, as described in Figure 15.

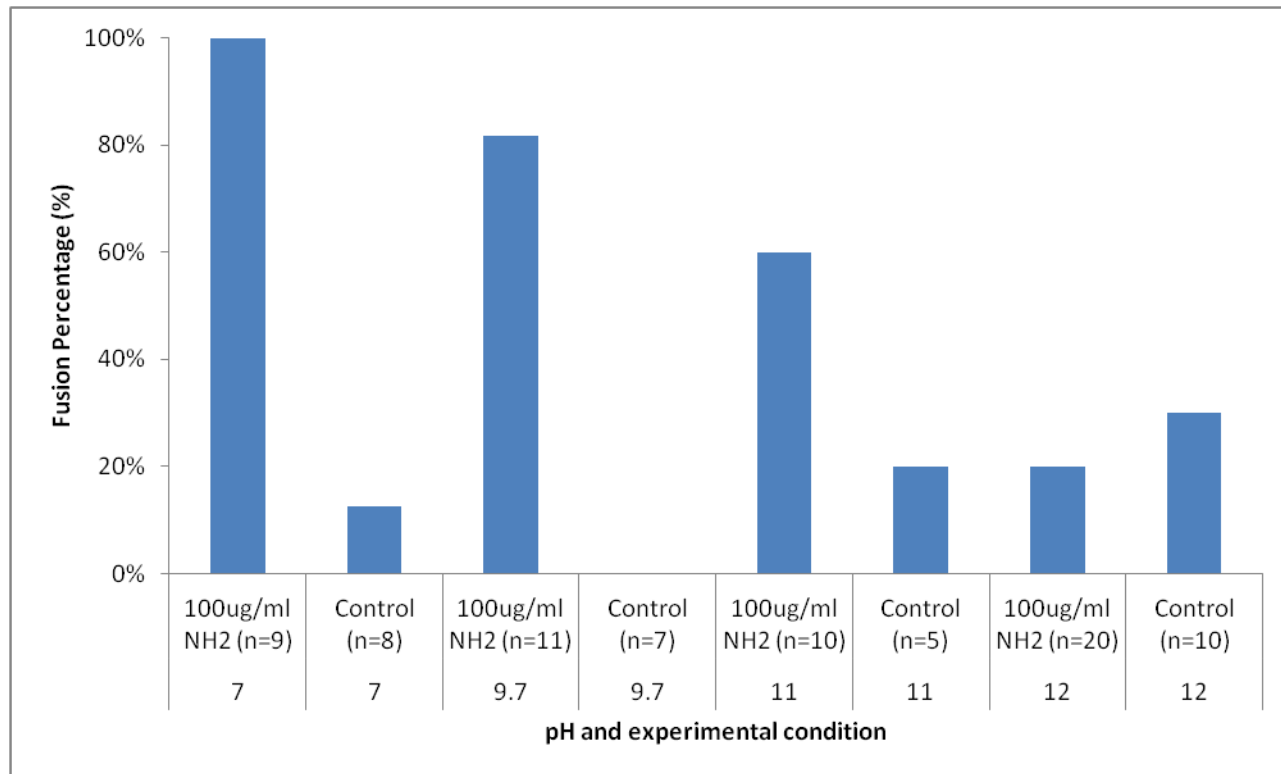


Figure 14. Bilayer fusion rates as a function of pH and experimental condition. As the pH increases, the number of wells that exhibit a fusion event decreases for the experimental group.

The results from Figure 15 are qualitatively very convincing. It is clear that there is a dependence on pH with the level of interaction with the plasma membrane conditions excluding

pH. It is important to always characterize the results relative to a control group. As the pH increases, the difference between the experimental group and control group greatly diminishes. Interestingly, as the pH increases, the fusion rate of control wells increases but the rate decreases for the experimental wells. In the case of the pH 12 experiment, there is no difference noted between the control and experimental group while the pH 7 experimental group had profound differences; thus, it appears that pH plays a significant role on nanoparticle interaction characteristics.

Shortly after, a glycosphingolipid, Cerebroside (CB), was added as it was an additional lipid found to be present in plasma membranes. By adding the Cerebroside, the bilayers became much easier to form. The sensitivity of these bilayers became such that by adding or removing small volumes of buffer solution to the bottom well, active control of the bilayer size could be performed. For example, if the protocol for bilayer formation was used and a particular membrane's capacitive current was too large, i.e. a bilayer was too large and produced too much noise, a small amount of buffer solution could be removed from the bottom well and reduce the hydrostatic pressure. This would then reduce the contact area of the two monolayers and thus reduce the size of the bilayer. This level of control was pivotal for high bilayer yield experiments and a breakthrough for our platform to consistently create experiments with near 100% bilayer formation yield. This level of sensitivity was important because it would allow the protocols to be more precise and push the bilayer yield to its maximum potential. An example where bilayer size would be important would be in reducing the size of the bilayer to reduce the noise associated with the membrane for single-channel studies.

The final lipid compositions used for high-yield bilayers that represent physiologically relevant conditions are described in Table 9.

Table 9. The most recently established composition of the plasma and lysosomal membranes on the basis of molar ratios of various lipids.

Lipid Composition	Molar Ratio Composition	
	Plasma Membrane	Lysosomal Membrane
Phosphatidylcholine (PC)	3	3
Phosphatidylethanolamine (PE)	1	1
Phosphatidylserine (PS)	1	1
Cholesterol (Chol)	1	1
Cerebroside (CB)	1	1
Bis(Monoacylglycero)Phosphate (BMP)	0	1

In addition to the specific lipid compositions, the aqueous solutions were also closely picked to follow those found in cellular conditions as shown in table 10.

Table 10. Aqueous buffer solution compositions for the plasma and lysosomal membranes.

	Plasma Membrane	Lysosomal Membrane
Sodium Chloride (NaCl)	150mM	80mM
Hepes (Buffering Agent)	4mM	0
Tris-HCL (Buffering Agent)	0	5mM
pH	7.0	4.5

Concluding the plasma membrane studies, it was clear that the amine-modified nanoparticles interact with the plasma membrane but the conditions needed for this interaction to occur required high concentrations of nanoparticles or low ionic strength aqueous solutions. Previous studies have suggested an interaction between the lysosomal membrane and these amine-modified nanoparticles. The reduced ionic strength and lower pH within the lysosomal membrane seem to suggest a more likely environment where these particles could interact electrostatically and at lower concentrations. The carboxyl-modified nanoparticles failed to interact in any significant way with the plasma membranes under physiologically relevant conditions, confirming previous literature findings and adding confidence to the findings of our platform and experimental protocols.

5.3 High-Throughput Nanoparticle Studies

Recently, a library of various nanoparticles has become available for testing and preliminary results have been included to illustrate the large data sets and statistically powerful data from these experiments.

The first nanoparticle to be investigated was the spherical fullerene, C_{60} . This particular nanoparticle has been suggested to be used as an x-ray contrast agent, a bone tissue target and as an antioxidant drug for neurodegenerative disease [30]. There is a need for a fundamental understanding of how C_{60} interacts with biological membranes which can be quickly observed through experimentation with the plasma membrane. When the C_{60} was tested using the plasma membrane conditions it was quickly evident that 100ug/ml would be very cytotoxic. The fantastic control group further signifies the strength of the platform when testing new nanoparticles and adds significance to the data, as observed in Figure 16. By altering the nanoparticle concentration, cytotoxicity studies can be quickly performed to look at the feasibility of the previously mentioned potential C_{60} nanoparticle applications.

February 28, 2014 S.C. C60 100ug/ml Duration: 150 minutes (2.5 hours)						
CONCLUSION: A few bilayers fused before adding NP's; however, no controls fused throughout the experiment after NP's were added and most of the C60 wells fused.						
No time to fusion because I forgot to write down exactly when I added NP's. Still a very obvious difference between control and experimental results.***						
Conditions	Particle	Wells Tested	Interaction	Fused	Comments	Time to fusion (min)
S.C. 150mM NaCl, 4 mM HEPES, pH 7.0	Control	7	1/7	0/7	Good control group. Only 1 well showed any noise/leak.	
S.C. 150mM NaCl, 4 mM HEPES, pH 7.0	C60 100ug/ ml	12	6/12	10/12	Many of the fusions occurred after a small increase in currents	***

Figure 15. Preliminary experimentation with C60 nanoparticles under plasma membrane conditions.

Another nanoparticle, Gadolinium Oxide (Gd_2O_3) also exhibited interesting results in both the plasma membrane and lysosomal membrane. These nanoparticles have a potential application as a contrasting agent in magnetic resonance imaging (MRI). The data compiled from the two preliminary experiments are shown in Figures 17 and 18.

April 7, 2014 S.C. Gd₂O₃ 500ug/ml
 Duration: 120 minutes (2 hours)

CONCLUSION: Very obvious interaction observed here and even a few consistent interaction spikes noted on the experimental wells (a few).

Conditions	Particle	Wells Tested	Interaction	Fused	Comments	Time to fusion (min)
S.C. 80mM NaCl, 5mM Tris-HCL pH 7.0	Control	7	1/7	0/7	Very large bilayers with stable flat currents, most 0pA and only a few below 10pA	--
S.C. 80mM NaCl, 5mM Tris-HCL pH 7.0	Gd ₂ O ₃ 500ug/ ml	8	6/8	6/8	A few consistent large interaction spikes observed a few minutes after adding particles.	39,66,71,80,93 ,94

Figure 16. Gd₂O₃ nanoparticle preliminary experiment data showing strong signs of interaction under plasma membrane conditions.

April 4, 2014 S.C.+BMP Gd ₂ O ₃ 500ug/ml Duration: 120 minutes (2 hours)						
CONCLUSION: Very obvious difference between control group and experimental group. The bilayers were very good and large.						
Conditions	Particle	Wells Tested	Interaction	Fused	Comments	Time to fusion (min)
S.C. +BMP Lysosomal conditions 80mM NaCl, 5mM Tris-HCL pH 4.5	Control	8		0/8	Very large bilayers with stable flat currents, most 0pA and only a few below 10pA	
S.C. +BMP Lysosomal conditions 80mM NaCl, 5mM Tris-HCL pH 4.5	Gd ₂ O ₃ 500ug/ ml	11	0/11	11/11	All fused very quickly except well 5 but it fused eventually	2,2,2,2,2,2,2, 2,4,21

Figure 17. Gd₂O₃ nanoparticles exhibiting strong signs of interaction under lysosomal membrane conditions.

Further experiments using various nanoparticles would yield results that indicate no interaction between both plasma membrane and lysosomal membrane conditions. This is still a positive result because it adds to the knowledgebase surrounding these seemingly limitless types of nanoparticles. More importantly, these tests help to quickly identify which nanoparticles are cytotoxic and, when examined more closely, variables such as pH, ionic strength, nanoparticle concentration and other factors can be examined quickly and efficiently with a high degree of confidence. Preliminary experiments on a few more nanoparticles have been included for reference and illustration of the high-throughput capabilities of the platform in Figures 19-24.

March 18, 2014 S.C. Pt NP's (30nm) 100ug/ml
Duration: 240 minutes(4 hours)

CONCLUSION: Very large bilayers and a great experiment. There was no obvious difference between the experimental and control group during this experiment. Minimal leak and noise currents. Very solid conclusion here.

Conditions	Particle	Wells Tested	Interaction	Fused	Comments	Time to fusion (min)
S.C. 150mM NaCl, 4 mM Hepes, pH 7.0	Control	7	1/7	0/7	Good control group. Only 1 well showed any noise/leak.	--
S.C. 150mM NaCl, 4 mM Hepes, pH 7.0	PtNP (30nm) 100ug/ ml	11	4/11	0/11	Interaction currents look similar to that of the control group.	--

Figure 18. Platinum nanoparticles of 30nm diameter under plasma membrane conditions exhibit no significant signs of interaction events.

March 19, 2014 S.C. Pt NP's (5nm) 100ug/ml
 Duration: 120 minutes(2 hours)

CONCLUSION: Bin already looked at the data (the files are missing somehow) and said there was no difference between the control and experimental groups.

Conditions	Particle	Wells Tested	Interaction	Fused	Comments	Time to fusion (min)
S.C. 150mM NaCl, 4 mM Hepes, pH 7.0	Control	7	0/7	0/7	Nothing really going on here. Good control group.	--
S.C. 150mM NaCl, 4 mM Hepes, pH 7.0	PtNP (5nm) 100ug/ ml	13	0/13	1/13	Nothing different from the control group observed.	93

Figure 19. Platinum nanoparticles of 5nm diameter under plasma membrane conditions exhibit no significant signs of interaction events.

March 19, 2014 S.C. + BMP (lysosomal conditions) Pt NP's (5nm) 100ug/ml
 Duration: 120 minutes(2 hours)

CONCLUSION: Bin already looked at the data (the files are missing somehow) and said there was no difference between the control and experimental groups.

Conditions	Particle	Wells Tested	Interaction	Fused	Comments	Time to fusion (min)
S.C.+BMP 80mM NaCl, 5 mM TRIS-HCL, pH 4.5	Control	8	0/8	0/8	Great control group.	--
S.C.+BMP 80mM NaCl, 5 mM TRIS-HCL, pH 4.5	PtNP (5nm) 100ug/ ml	15	2/15	0/15	Transient spikes right after adding NP's in 1 well and another about 8 minutes later.	--

Figure 20. Platinum nanoparticles of 5nm diameter under lysosomal membrane conditions exhibit no significant signs of interaction events.

March 20, 2014 S.C. + BMP (lysosomal conditions) Pt NP's (30nm) 100ug/ml
 Duration: 150 minutes(2.5 hours)

CONCLUSION: After 2.5 hours, the controls are great and no current above 10pA and very large bilayers. The experimental group had 2/15 fuse and has shown a few currents which are consistent over a few wells. It is possible this concentration is too low to establish an observable effect.

Conditions	Particle	Wells Tested	Interaction	Fused	Comments	Time to fusion (min)
S.C.+BMP 80mM NaCl, 5 mM TRIS-HCL, pH 4.5	Control	9	1/9	0/9	Great control group.	--
S.C.+BMP 80mM NaCl, 5 mM TRIS-HCL, pH 4.5	PtNP (30nm) 100ug/ ml	15	4/15	2/15	A few wells showing interesting currents but very little interaction observed.	1,51

Figure 21. Platinum nanoparticles of 30nm diameter under lysosomal membrane conditions exhibit no significant signs of interaction events.

March 21, 2014 S.C. + BMP (lysosomal conditions) Pt NP's (30nm) 100ug/ml Duration: 300 minutes (5 hours) Repeated experiment from March 20,2014*** CONCLUSION: Similar results to the original experiment and all the bilayers were stable and did not show any currents aside from 2 of the Pt bilayers. These were not consistent with the previous day so it looks like there is no different between the control group and experimental group at this concentration and under these conditions.						
Conditions	Particle	Wells Tested	Interaction	Fused	Comments	Time to fusion (min)
S.C.+BMP 80mM NaCl, 5 mM TRIS-HCL, pH 4.5	Control	9	0/9	0/9	Great control group.	--
S.C.+BMP 80mM NaCl, 5 mM TRIS-HCL, pH 4.5	PtNP (30nm) 100ug/ml	15	2/15	0/15	Does not seem to be any interaction.	--

Figure 22. Repeated experiment confirming platinum nanoparticles of 30nm diameter under lysosomal membrane conditions do not exhibit any significant sign of interaction events.

April 1, 2014 S.C. + BMP (lysosomal conditions) FeO ₂ 100ug/ml Duration: 120 minutes(2.0 hours)						
CONCLUSION: Great experiment. 95% bilayer yield and great control group. Large bilayers observed and possible interaction observed in the control group but very short-lived and would probably need a higher concentration to see any obvious effect.						
Conditions	Particle	Wells Tested	Interaction	Fused	Comments	Time to fusion (min)
S.C.+BMP 80mM NaCl, 5 mM TRIS-HCL, pH 4.5	Control	7	2/7	0/7	Great control group. The currents observed were very small and transient	--
S.C.+BMP 80mM NaCl, 5 mM TRIS-HCL, pH 4.5	PtNP (30nm) 100ug/ml	15	7/15	0/15	Possible interaction. Further testing needed.	--

Figure 23. Preliminary experiment with iron oxide nanoparticles may show possible interaction events under lysosomal membrane conditions.

These preliminary experiments were highly valuable in characterizing our platforms ability to repeatedly conduct large-scale experiments with incredibly high bilayer formation rates. The amine-modified and carboxyl-modified nanoparticles are essentially just the tip of the iceberg within the extensive list of possible nanoparticles to be tested. Examining the effect of varying ionic strength, pH and lipid composition allows an exhaustive list of variables to be tested for each nanoparticle and elicits a strong chance for uncovering the biological mechanism for interaction events. The scalability of the bilayer arrays in this platform is only limited to the number of available channels on the amplifier and available resources. In the future, this system

could become completely automated, reducing the variability between operators and allowing for tighter regulations within the experimental protocols.

Chapter 6: Conclusions

In conclusion, traditional methods in artificial bilayer reconstitution have been slow to meet the needs of growing demands in medical research. Hence, the need has arisen for a platform that can quickly and accurately investigate physiologically relevant artificial bilayers under a large range of conditions. The improved platform fabrication and artificial bilayer reconstitution methods have drastically improved the feasibility to produce high-throughput bilayers that mimic the plasma and lysosomal membrane conditions. The recent nanoparticle studies have shown the statistical power of the platform to analyze large data sets. More specifically, the studies involving amine-modified and carboxyl-modified polystyrene nanoparticles have shown similar results as other studies performed by traditional methods. Our platform has been able to investigate the effects of pH, ionic strength and various lipid combinations to further the depth of investigation of these nanoparticles. From these results, we have suggested an electrostatic interaction as the primary means of interaction between the nanoparticles and plasma and lysosomal membranes. Recently, we have used the high-throughput aspect of our platform extensively to investigate a library of nanoparticles to quickly discern the likelihood of passive interaction between plasma and lysosomal membranes. The platinum nanoparticles have not shown any interaction under any of the membrane conditions tested. Iron oxide nanoparticles have shown possible interactions under lysosomal conditions but more testing is needed to quantify these potential interactions. Fullerene C60 particles have also shown a strong interaction within plasma membranes. Additionally, the gadolinium oxide nanoparticles interacted very strongly with both the lysosomal and plasma membranes. More experimentation is needed to test the significance of pH, ionic strength and particle concentration to determine the nature of this particles interaction. The development of a standard protocol to

accurately represent both the plasma membrane and lysosomal membrane conditions has improved the efficacy of nanoparticle screening.

Chapter 7: Future Applications

7.1 Nanoparticle Screening

The impressive potential of nanoparticles in modern medicine is only eclipsed by the number of combinations of conditions they can be tested in. The current platform is suitable for studying the effect of nanoparticles on passive interaction between nanoparticles on either plasma membranes or lysosomal membranes. In the future, including more physiologically relevant membrane conditions such as the mitochondrial membrane and more complex lipid compositions which more closely relate to those found in cells would be advantageous to examining the interactions. In many cases, there is no obvious interaction shown when utilizing the plasma membrane or lysosomal membrane conditions yet the nanoparticles may still be cytotoxic via another interaction, possibly with another membrane system or via an active method. Further investigation into how more complex membrane conditions like these can be quickly and efficiently established using the current platform would greatly improve the viability of this high-throughput platform. By cycling through various experimental conditions involving pH, ionic strength, membrane conditions and particle concentration using a wide variety of nanoparticles, we hope to quickly and efficiently examine a large library of available nanoparticles.

7.2 Nanopore Sequencing

In today's technological age there has been an overwhelming push to revolutionize the world of medicine. Through the invention of DNA sequencing, the standpoint of medical treatment has now potentially become one of treating an ailment before it even exists. There are more than seven billion people on the planet, each with a unique DNA code (excluding identical twins) that separates them from anyone on the planet. This DNA code is a set of instructions that

dictates all the information required for every cell in the body to function. The structure of DNA was famously first described in 1953 by Watson & Crick as a double helix structure [31]. As DNA is replicated, mistakes are made every so often that change the message encoded. The human body is very good at keeping track of this process but every now and then a mistake gets through the checkpoints. Occasionally, even one change to a single nucleotide can have a drastic change, as is the case of sickle cell disease. This rare disease mutates the shape of red blood cells causing them to take on a sickle shape which drastically changes the flexibility of the red blood cells and causes a shortened lifespan; however, if the person is just a carrier of the sickle-cell trait, they will only mildly have these symptoms and will lead a relatively normal life. Diseases like this and many others clearly display the importance of understanding the impact of sequencing and subsequently the changes in healthcare and treatments options to every-day people.

As genomic sequencing becomes more available, this information can be used to design drugs targeted at specific physiological pathways to a specific disease. If the drug is more specific, there are fewer side effects that can decrease the effectiveness of the treatment. This new era of treatment will end the “one-size-fits-all” approach to pharmaceuticals and cancer treatments and will help bring a personalized approach to medicine for detecting, treating and ultimately preventing disease. The question is still unanswered as to how DNA is sequenced and, more importantly, how this relates to lipid bilayers.

In 2004, the NIH set an incredible challenge to scientists: the \$1000 genome. This would put genetic sequencing on the map as cost effective and affordable to the average consumer. Although technologies such as Sanger sequencing technique existed, it was unlikely to ever be cost effective and thus improvements needed to be made. According to Bayley’s group, only single-molecule sequencing approaches in parallel would be able to tackle the challenge put up

by the NIH [32]. Our platform is capable of producing single protein ion channels but further research needs to be conducted to create a protocol for consistent single-channel bilayers in parallel arrays. Ion channels such as MspA [33] and Alpha-Hemolysin [34] have been shown to reliably sequence DNA. These proteins can be incorporated into massive arrays of bilayers and sequencing time and cost could be drastically reduced. Although these two ion channels are effective in relating nucleotide bases into current readouts, this method is still very limited. One challenge for the strand sequencing method is the resolution to be able to detect single nucleotide bases. The DNA strand moves so rapidly through the pore that it is incredibly difficult to discern the individual bases from one another. In addition, the data has been difficult to read because the current generated from the single molecular pore is so small that noise dominates the signal. In our platform, we have tested Alpha-Hemolysin and found it to be a relatively easy ion channel to work with; however, obtaining a single ion channel for any valuable length of time has proven to be difficult. The idea of adding an Alpha-Hemolysin inhibitor after confirmation of a single ion channel within the membrane has been postulated but has proved to be challenging to execute experimentally. Solution exchange experiments have been shown to be very effective on this platform but have not been tested in parallel. Solution exchange is a good method for removing the Alpha-Hemolysin proteins from solution but is difficult to execute in parallel because the single channels membranes would occur at different times throughout the experiment and would need to be exchanged based on the incorporation of the protein into each particular membrane. With further improvements, future applications involving large scale drug screening, nanoparticle studies and nanopore based DNA sequencing could be realized.

Appendix A. Protocols

Plasma membrane & amine-modified polystyrene nanoparticles (X^* ug/ml final concentration)
in physiologically relevant conditions

Super Combo (S.C.) – Refer to Table 4 for the lipid composition and molar ratios

1. Add 450uL to the bottom chamber at a concentration of 250ug/ml S.C. Liposome Solution
 - a. Buffer: 150mM NaCl, 4mM Hepes, pH 7.0
2. Add 25uL to the central well at a concentration of 10mg/ml S.C. dissolved in decane
 - a. Notes: Sometimes a precipitate can be seen in the decane/lipid solution. To fix this, place the amber vial between your hands to warm the vial to body temperature and then vortex until the lipid has fully dissolved.
3. WAIT 15 MINUTES.
 - a. Notes: During this time, the electrodes should be cleaned and then placed carefully into their corresponding positions on the platform. Adding the electrodes after step 4 can result in unintentional fusions.
4. Add 50uL of buffer to the central well.
 - a. Buffer: 150mM NaCl, 4mM Hepes, pH 7.0
 - b. Notes: It is important to carefully and slowly add the buffer solution to the central with a steady hand and a watchful eye of the electrodes. Disturbing the electrodes could unintentionally disrupt the bilayer formation.
5. Add 50uL to the bottom chamber at a concentration of 250ug/ml S.C. Liposome Solution
 - a. Buffer: 150mM NaCl, 4mM Hepes, pH 7.0
 - b. Notes: This step should be repeated for wells that have a capacitive current below the standard of 180pA during the applied triangle wave protocol. This step is

slightly subjective and, over time, the capacitive current will grow as the bilayers become larger.

6. Switch the voltage protocol to the triangle wave and subsequent constant voltage sweeps of +/- 70mV.
7. Wait until the bilayers have formed, taking careful note of any bilayers that do not form properly or exhibit any non-zero resistive currents (leak or noise).
8. WAIT AT LEAST 10 MINUTES to confirm bilayer formation and assess stability.
9. Add 5.5uL of (10X) mg/ml NH₂-PS nanoparticles carefully into the central well for the experimental group and add 5.5uL of the buffer solution used in the experiment for the control group.
 - a. Notes: Always have at least 1/3 of the wells from each chip be control wells (minimum 2 wells, preferably 3 or 4).
 - i. Note the time the solutions were added to the wells and the corresponding wells as control or experimental group

*The desired concentration, X, will be 10 times less than the concentration added to the central well during step 9. For example, a desired final concentration of 100ug/ml would require the addition of 1mg/ml of stock nanoparticle solution into the central well during step 9.

Lysosomal membrane & amine-modified polystyrene nanoparticles (X ug/ml final concentration) in physiologically relevant conditions

Super Combo + BMP (S.C. +BMP) – Refer to Table 4 for the lipid composition and molar ratios

1. Add 450uL to the bottom chamber at a concentration of 250ug/ml S.C. +BMP Liposome Solution
 - a. Buffer: 80mM NaCl, 5mM Tris-HCL, pH 4.5
2. Add 25uL to the central well at a concentration of 10mg/ml S.C.+BMP dissolved in decane
 - a. Notes: Sometimes a precipitate can be seen in the decane/lipid solution. To fix this, place the amber vial between your hands to warm the vial to body temperature and then vortex until the lipid has fully dissolved.
3. WAIT 15 MINUTES.
 - a. Notes: During this time, the electrodes should be cleaned and then placed carefully into their corresponding positions on the platform. Adding the electrodes after step 4 can result in unintentional fusions.
4. Add 50uL of buffer to the central well.
 - a. Buffer: 80mM NaCl, 5mM Tris-HCL, pH 4.5
 - b. Notes: It is important to carefully and slowly add the buffer solution to the central with a steady hand and a watchful eye of the electrodes. Disturbing the electrodes could unintentionally disrupt the bilayer formation.
5. Add 50uL to the bottom chamber at a concentration of 250ug/ml S.C.+BMP Liposome Solution
 - a. Buffer: 80mM NaCl, 5mM Tris-HCL, pH 4.5

- b. Notes: This step should be repeated for wells that have a capacitive current below the standard of 180pA during the applied triangle wave protocol. This step is slightly subjective and, over time, the capacitive current will grow as the bilayers become larger.
6. Switch the voltage protocol to the triangle wave and subsequent constant voltage sweeps of +/- 70mV.
7. Wait until the bilayers have formed, taking careful note of any bilayers that do not form properly or exhibit any non-zero resistive currents (leak or noise).
8. WAIT AT LEAST 10 MINUTES to confirm bilayer formation and assess stability.
9. Add 5.5uL of (10X)mg/ml NH₂-PS nanoparticles carefully into the central well for the experimental group and add 5.5uL of the buffer solution used in the experiment for the control group.
 - a. Notes: Always have at least 1/3 of the wells from each chip be control wells (minimum 2 wells, preferably 3 or 4).
 - i. Note the time the solutions were added to the wells and the corresponding wells as control or experimental group

*The desired concentration, X, will be 10 times less than the concentration added to the central well during step 9. For example, a desired final concentration of 100ug/ml would require the addition of 1mg/ml of stock nanoparticle solution into the central well during step 9.

References

1. Salata, O., *Applications of Nanoparticles in Biology and Medicine*. Journal of Nanobiotechnology, 2004.
2. Lundqvist, M., *Nanoparticles: Tracking protein corona over time*. Nat Nanotechnol, 2013. **8**(10): p. 701-2.
3. Nicholson, S.J.S.G.K., *The Fluid Mosaic Model of The Structure of Cell Membranes*. Science, 1972: p. 720-731.
4. Schlue, W.H.W.-R., *Planar Lipid Bilayers*, ed. D. Sattelle. 1993: Academic Press.
5. Gest, H., *The discovery of microorganisms by Robert Hooke and Antoni Van Leeuwenhoek, fellows of the Royal Society*. Notes Rec R Soc Lond, 2004. **58**(2): p. 187-201.
6. Mueller, P., et al., *Reconstitution of Excitable Cell Membrane Structure in Vitro*. Circulation, 1962. **26**(5): p. 1167-1171.
7. M. Montal, P.M., *Formation of Biomolecular Membranes from Lipid Monolayers and a Study of Their Electrical Properties*. Proceedings of the National Academy of Sciences, 1972.
8. White, S.H., *The Physical Nature of Planar Bilayer Membranes*. 1986.
9. Miller, C., *Ion Channel Reconstitution*. 1986. 115-130.
10. Sakmann, E.N.B., *Single Channel Recording*. 1983: Plenum Press.
11. Takeuchi, S., *Lipid Bilayer Microarray for Parallel Recording of Transmembrane Ion Currents*. Analytical Chemistry, 2008.
12. Suzuki, H., B. Le Pioufle, and S. Takeuchi, *Ninety-six-well planar lipid bilayer chip for ion channel recording fabricated by hybrid stereolithography*. Biomed Microdevices, 2009. **11**(1): p. 17-22.
13. Takeuchi, S., *Lipid Bilayer Formation by Contacting Monolayers in a Microfluidic Device for Membrane Protein Analysis*. Analytical Chemistry, 2006.
14. Babakov, A.V., *Production of Biomolecular Protein-Lipid Membranes in Aqueous Solution*. Nature, 1966.
15. Bayley, H., *Functional Bionetworks from Nanoliter Water Droplets*. Journal of the American Chemical Society, 2007.
16. Bayley, H., et al., *Droplet interface bilayers*. Mol Biosyst, 2008. **4**(12): p. 1191-208.

17. Aghdaei, S., et al., *Formation of artificial lipid bilayers using droplet dielectrophoresis*. Lab Chip, 2008. **8**(10): p. 1617-20.
18. Poulos, J.L., et al., *Electrowetting on dielectric-based microfluidics for integrated lipid bilayer formation and measurement*. Applied Physics Letters, 2009. **95**(1): p. 013706.
19. Poulos, J.L., et al., *Ion channel and toxin measurement using a high throughput lipid membrane platform*. Biosens Bioelectron, 2009. **24**(6): p. 1806-10.
20. Kawano, R., et al., *Automated parallel recordings of topologically identified single ion channels*. Sci Rep, 2013. **3**: p. 1995.
21. Lu, B., G. Kocharyan, and J.J. Schmidt, *Lipid bilayer arrays: Cyclically formed and measured*. Biotechnology Journal, 2014. **9**(3): p. 446-451.
22. El-Arabi, A.M., C.S. Salazar, and J.J. Schmidt, *Ion channel drug potency assay with an artificial bilayer chip*. Lab Chip, 2012. **12**(13): p. 2409-13.
23. Portonovo, S.A. and J. Schmidt, *Masking apertures enabling automation and solution exchange in sessile droplet lipid bilayers*. Biomed Microdevices, 2012. **14**(1): p. 187-91.
24. Gregorova, W.P.E., *Characterization of Particles and Particle Systems*. 2007: p. 29-30.
25. Merkus, H.G., *Particle Size Measurements: Fundamentals, Practice, Quality*. 2009: Springer Science+Business Media B.V.
26. Agasti, S.S., et al., *Nanoparticles for detection and diagnosis*. Adv Drug Deliv Rev, 2010. **62**(3): p. 316-28.
27. Wang, F., et al., *Time resolved study of cell death mechanisms induced by amine-modified polystyrene nanoparticles*. Nanoscale, 2013. **5**(22): p. 10868-76.
28. Ekkapongpisit, M., et al., *Biocompatibility, endocytosis, and intracellular trafficking of mesoporous silica and polystyrene nanoparticles in ovarian cancer cells: effects of size and surface charge groups*. Int J Nanomedicine, 2012. **7**: p. 4147-58.
29. van Meer, G., D.R. Voelker, and G.W. Feigenson, *Membrane lipids: where they are and how they behave*. Nat Rev Mol Cell Biol, 2008. **9**(2): p. 112-24.
30. D'Rozario, R.S., et al., *The interaction of C60 and its derivatives with a lipid bilayer via molecular dynamics simulations*. Nanotechnology, 2009. **20**(11): p. 115102.
31. Crick, J.D.W.F.H.C., *Molecular Structure of Nucleic Acids*. Nature, 1953. **171**: p. 737-738.
32. Bayley, H., *Sequencing single molecules of DNA*. Curr Opin Chem Biol, 2006. **10**(6): p. 628-37.

33. Manrao, E.A., et al., *Reading DNA at single-nucleotide resolution with a mutant MspA nanopore and phi29 DNA polymerase*. Nat Biotechnol, 2012. **30**(4): p. 349-53.
34. Stoddart, D., et al., *Single-nucleotide discrimination in immobilized DNA oligonucleotides with a biological nanopore*. Proc Natl Acad Sci U S A, 2009. **106**(19): p. 7702-7.